Assessing Challenging Intra-and Inter-Molecular Charge-Transfer Excitations Energies with Double-Hybrid Density Functionals

Éric Brémond, Alistar Ottochian, Ángel José Pérez-Jiménez, Ilaria Ciofini, Giovanni Scalmani, Michael Frisch, Juan Carlos Sancho-García, Carlo Adamo

Assessing Challenging Intra- and Inter-Molecular Charge-Transfer Excitations Energies with Double-Hybrid Density Functionals

Journal:	*Journal of Computational Chemistry*
Manuscript ID	Draft
Wiley - Manuscript type:	Full Paper
Date Submitted by the Author:	n/a
Complete List of Authors:	Brémond, Éric; Université de Paris Ottochian, Alistar; PSL Research University, Chimie Paristech-CNRS, Institut de Recherche de Chimie de Paris Pérez-Jiménez, Ángel; Universidad de Alicante, Química-Física Ciofini, Ilaria; ENSCP - Chimie Paristech, ICLeHs FRE2027 Scalmani, Giovanni; Gaussian, Inc Frisch, Micheal; Gaussian, Inc. Sancho-Garcia, Juan Carlos; University of Alicante, Physical Chemistry Adamo, Carlo; PSL Research University, Chimie Paristech-CNRS, Institut de Recherche de Chimie de Paris
Key Words:	TD-DFT, Charge-Transfer Excitation Energies, Double-Hybrid Density Functional, Weakly Bound Complexes

Assessing Challenging Intra- and Inter-Molecular Charge-Transfer Excitations Energies with Double-Hybrid Density Functionals

E. Brémond[a]*, A. Ottochian[b], A.J. Pérez-Jiménez[c], I. Ciofini[b], G. Scalmani[d], M. J. Frisch[d], J. C. Sancho-García[c]†, and C. Adamo[b,e]‡

[a] Université de Paris, ITODYS, CNRS, F-75006 Paris, France

[b] Chimie ParisTech, PSL Research University, CNRS, Institute of Chemistry for Life and Health Sciences (i-CLeHS), FRE 2027, F-75005 Paris, France

[c] Department of Physical Chemistry, University of Alicante, E-03080 Alicante, Spain

[d] Gaussian, Inc., Wallingford, 340 Quinnipiac, St., Bldg. 40, Wallingford, CT 06492, USA

[e] Institut Universitaire de France, 103 Boulevard Saint Michel, F-75005 Paris, France

*E-mail: eric.bremond@u-paris.fr
†E-mail: jc.sancho@ua.es
‡E-mail: carlo.adamo@chimie-paristech.fr

Abstract

We investigate the performance of a set of recently introduced range-separated double-hybrid functionals, namely ωB2-PLYP, ωB2GP-PLYP, RSX-0DH, and RSX-QIDH models for hard-to-calculate excitation energies. We compare with the parent (B2-PLYP, B2GP-PLYP, PBE0-DH, and PBE-QIDH) and other (DSD-PBEP86) double-hybrid models as well as with some of the most widely employed hybrid functionals (B3LYP, PBE0, M06-2X, and ωB97X). For this purpose, we select a number of medium-sized intra- and inter-molecular charge-transfer excitations, which are known to be challenging to calculate using TD-DFT and for which accurate reference values are available. We assess whether the high accuracy shown by the newest double-hybrid models is also confirmed for those cases too. We find that asymptotically corrected double-hybrid models yield a superior performance, especially for the inter-molecular charge-transfer excitation energies, as compared to standard double-hybrid models. Overall, the PBE-QIDH and its corresponding range-separated RSX-QIDH functional are recommended for general-purpose TD-DFT applications, depending on whether long-range effects are expected to play a significant role.

1 Introduction

The description of electronically excited-states by Time-Dependent Density-Functional Theory (TD-DFT) has become increasingly accurate and robust in recent years. One of the main reasons for this is its appealing trade-off between accuracy and computational cost for standard systems and common applications while the adiabatic approximation still precludes its application to more complicated molecular excitations like doubly-excited states. However, TD-DFT leverages the lessons learned from extensive ground-state applications and benchmark studies; among them, and particularly relevant for this work, the higher accuracy and robustness of Double-Hybrid (DH) models as compared to Global-Hybrid (GH) density functionals, demonstrated for many chemically meaningful applications,[1–18] and rooted in both the quality of the approximation of the exchange-correlation energy, and the underlying modern hybridization scheme.[19] Therefore, for most common TD-DFT applications, the accuracy of excited-state calculations strongly depends on the adequate selection of the underlying exchange-correlation functional, for which comparable benchmark studies beyond those extensively done for ground-state properties are still lacking. Generally speaking, the benchmarking of DH functionals made in recent years, although focused mainly for vertical excitation energies of organic compounds, has nevertheless led to establish that DH models outperform the corresponding hybrid ones for excitation energies[20–28] albeit still leaving much room for further improvement.[29,30]

Of particular interesting is the longstanding goal of improving long-range properties without deteriorating the whole accuracy of the models.[31–33] In this regard, a range-separation strategy has also been adopted recently

for double-hybrid functionals, with the range-separation parameter tuned for ground-state applications[34,35] or directly obtained from model systems, and thus without resorting to any parameterization, namely as in the RSX scheme.[36–38] An important step further has been the recent extension of exchange range-separation by Goerigk *et al.*,[39] specifically fitting the range-separation parameter ω (or, in other works, μ) in the pair of double-hybrid functionals ωB2-PLYP and ωB2GP-PLP, to reproduce reference excitation energies as closely as possible. The pioneering applications to singlet-singlet and singlet-triplet transitions were very promising,[40] with or without the Tamm-Dancoff approximation.[41] Thus, it seems also appropriate to extend this kind of range-separated DH functional to the calculation of challenging excited-state properties, which will be systematically explored in this work using the RSX-0DH and RSX-QIDH methods. For this assessment of recent developments with double-hybrid functionals, we have selected a set of singlet-singlet ($S_1 \leftarrow S_0$) excitations in weakly bound inter-molecular charge-transfer (CT) complexes, as examples of complicated excitations characterized by strong long-range nature.[42] These donor-acceptor dimers are non-covalently bound with equilibrium distances generally found to be around $3.2 - 3.6$ Å, making them attractive as challenging cases.[43]

The interest of studying inter-molecular CT excitations is far from being only conceptual or a motivation to foster methods development. In the field of organic electronics, these states are formed at the interface between the electron-donor and electron-acceptor materials and drive the processes of exciton dissociation, charge-separation and/or charge-recombination, which are key for the performance of photoactivated systems or organic solar cells.[44–46] The dynamic nature of the bulk and the organic-organic interface

of functional organic materials make difficult to rely on geometry- and/or system-dependent parametrizations, thus motivating the search for reliable and general-purpose computational methods. The same applies to biomolecular applications, where the interplay of valence and CT excitations also controls the excited-state dynamics of these systems.[47–49]

For this work, we selected the weakly bound complexes shown in Figure 1, i.e., the set formed by tetracyanoethylene (TCNE) and a polycyclic aromatic hydrocarbon (i.e., benzene, toluene, *o*-xylene, naphtalene, hexamethylbenzene, and diphenylene) as well as the hexamethylbenzene-chloranil and diphenylene-chloranil dimers.[50,51] We will also extend the study to a set of intra-molecular CT excitations, arising from intra-molecular donor-acceptor interactions involving by the coumarin-152, DCS (4-dimethylamino-4'-cyano-stilbene), and DANS (4-dimethylamino-4'-nitro-stilbene) push-pull dyes, and we will include an example of CT excitation energies at infinite separation for the ammonia-fluorine complex. We will also consider a set of radical (open-shell) small molecular systems, taken from the last work of Loos *et al.*,[52] to assess for the first time the performance of TD-DFT with DH methods for doublet-doublet ($D_1 \leftarrow D_0$) transitions in BH_2, HCO, HOC, H_2PO, H_2PS, NH_2, and PH_2. We note that luminescent organic radicals are also being recently investigated as active emitters in organic light-emitting diodes (OLED) to circumvent the difficulty in harvesting triplet excitons, typical of closed-shell emitters.[53,54] Since DH functionals are being progressively and successfully implemented in widely used codes,[55,56] we hope this assessment will further stimulate both the development and the use of such methods for excited-state applications, as their accuracy for all kind of excitation energies is confirmed.

2 Theoretical Methods

We start by recalling the expression of a global hybrid (GH) density functional:

$$E_{xc}^{GH}[\rho] = a_x E_x^{EXX}[\phi_i] + (1 - a_x)\, E_x[\rho] + E_c[\rho], \tag{1}$$

where $E_x[\rho]$ and $E_c[\rho]$ are the exchange and correlation density functional approximations, and a_x the coefficient of the exact-exchange (EXX) term, E_x^{EXX}, which depends on the set of occupied orbitals $\{\phi_i\}$. The effort to improve the accuracy and robustness of density functional approximations has led to the development of double-hybrid (DH) models,[57–61] whose correlation density functional is now augmented with a second-order perturbation theory (PT2) term, which is a function also of the unoccupied orbitals $\{\phi_a\}$, and is included in the energy expression with a coefficient a_c:

$$E_{xc}^{DH}[\rho] = a_x E_x^{EXX}[\phi_i] + (1 - a_x)\, E_x[\rho] + a_c E_c^{PT2}[\phi_i, \phi_a] + (1 - a_c)\, E_c[\rho]. \tag{2}$$

Furthermore, a range-separation for the exchange term, which is a successful strategy to improve the asymptotic behavior of hybrid functionals, is introduced by splitting the electron-repulsion operator r_{ij}^{-1} using the error function:

$$\frac{1}{r_{ij}} = \frac{1 - [\alpha + \beta \operatorname{erf}(\omega r_{ij})]}{r_{ij}} + \frac{\alpha + \beta \operatorname{erf}(\omega r_{ij})}{r_{ij}}, \tag{3}$$

where α and $\alpha + \beta$ are coefficients used to weight the short- and long-range EXX, respectively, with the range-separation parameter ω governing the separation between the two regimes. In order to assess the performance of different DH models, we have selected the following functionals: B2-PLYP,[62] ωB2-PLYP,[39] B2GP-PLYP,[63] ωB2GP-PLYP,[39] PBE0-DH,[64] RSX-0DH,[37] PBE-QIDH,[65] and RSX-QIDH.[36] Table 1 summarizes the a_x, a_c, and ω

values for these methods. We will also add, for completeness and cross-comparison, the DSD-PBEP86 spin-component scaled (SCS) model,[8,66,67] which is based on the PBEP86 semi-local exchange-correlation functional, but involves a separate (and scaled) contribution of the same- and opposite-spin correlation energy of the E_c^{PT2} term. Spin-component scaling is another strategy pursued in the development of DH models.[68,69] Indeed, DSD-PBEP86 was found to be one of the most accurate in a large study of of SCS double-hybrid functionals in TD-DFT applications.[30] We also selected a set of the most widely used hybrid functionals, including B3LYP,[70] PBE0,[71] M06-2X,[72] and ωB97X.[73]

In modern implementations of DH functionals in TD-DFT[74] the excitation energies (Ω) includes two components,

$$\Omega^{DH} = \Omega^{GH} + a_c \Delta\Omega^{(D)}, \tag{4}$$

where Ω^{GH} is the vertical excitation energy computed with the GH functional, and $\Delta\Omega^{(D)}$ is the perturbative correction to the Configuration Interaction Singles including Double excitations, CIS(D).[75] Note that in this approach the value of a_c from Eq. (2) is not modified and the correspoing terms still involves both the ground-state self-consistent occupied and virtual orbitals obtained using the underlying GH functional. The selection of DH functionals considered in this work is expected to shed light on: (i) the general accuracy of GH vs. DH models, both long-range corrected and not; (ii) the influence of the underlying exchange-correlation functional (e.g. PBE[76] for PBE0-DH and PBE-QIDH vs. BLYP[77,78] for B2-PLYP and B2GP-PLYP); (iii) the role of the a_x and a_c coefficients in the functional; (iv) the effect of the range-separation in the recently developed DH models like ωB2-PLYP and ωB2GP-PLYP vs B2-PLYP and B2GP-PLYP, respectively,

as well as RSX-0DH and RSX-QIDH vs. PBE0-DH and PBE-QIDH; and (v) the importance of the $a_c\Delta\Omega^{(D)}$ term, comparing results with and without it.

2.1 Computational Details

The molecular geometries for the CT complexes were taken from literature: benzene-TCNE, toluene-TCNE, *o*-xylene-TCNE, and naphtalene-TCNE are taken from Ref. 50; hexamethylbenzene-TCNE, diphenylene-TCNE, hexamethylbenzene-chloranil, and diphenylene-chloranil are taken from Ref. 51. We have used throughout the study the (aug-)cc-pV(D,T)Z basis sets,[79] to allow the adequate comparison with reference and literature results. Excitation energies with DH functionals can be considered nearly converged using a triple-ξ basis sets.[30] A development version of the GAUSSIAN'16 program[80] was used for all the calculations, with increased numerical thresholds (keywords: 'SCF=Tight', 'Int=Ultrafine'). The ORCA 4.2.1. release[81,82] with increased thresholds too (keywords: 'TightSCF', 'NoFinalGrid', 'Grid6') was also used for interfacing the results to the TheoDORE 2.2 program (*vide infra*). We employed the RIJCOSX technique[83] and the automatic generation of appropriate auxiliary basis sets.[84]

We computed the 'Mean-Signed Error' (MSE), the 'Mean Unsigned Error' (MUE), and the 'Root Mean-Squared Error' (RMSE) for all the methods assessed, respectively, as MSE $= \frac{1}{n}\sum_i^n x_i$, MUE $= \frac{1}{n}\sum_i^n |x_i|$, and RMSE $= \sqrt{\frac{1}{n}\sum_i^n x_i^2}$, with $x_i = \Omega_i^{\text{calculated}} - \Omega_i^{\text{reference}}$, as well as the maximum (MAX) individual deviation between calculated and reference values. We will consistently compare TD-DFT results obtained by DHs with accurate reference values, and when possible, such values would come from experiment.[85] However, in the case of CT excitations measured in solutions,

solvatochromic effects might be important and system-dependent, which makes difficult a direct comparison. Thus, in absence of gas-phase experimental results, we will compare our results with those obtained using highly correlated *ab initio* methods to avoid solvation and other geometrical and vibronic effects. Such accurate *ab initio* reference data are mostly SCS-CC2 quality[86,87] or obtained using higher-order methods (e.g., CCSDT-3). The SCS-CC2 might be considered not accurate enough for benchmark studies; however, according to recent work, such values are sufficiently close to other more costly methods[88–90] and their use is not expected to significantly influence the general conclusions that are going to be reached.

2.2 Identification of Charge-Transfer States

Considering the rather intricate nature of the excited-states for the systems considered and the variety of functionals used, a reliable definition of the charge-transfer character of the molecular excitations[91,92] is needed. The TheoDORE 2.2 program[93,94] was used for this purpose, through the analysis of the one-particle transition density matrix[95,96] which will also allow for the comparison with existing data. For the weakly bound (intermolecular) CT complexes, each of the weakly interacting molecules of the dimer is defined as a fragment to carry out the exciton analysis using the following descriptors:[97–99] (i) the average hole and electron (or exciton) position (Ω_{POS}) with a range from $\Omega_{\mathrm{POS}} = 1$ to $\Omega_{\mathrm{POS}} = 2$, with both limits corresponding to local excitations localized on one or the another fragment, and thus $\Omega_{\mathrm{POS}} \approx 1.5$ indicating a pure CT transition; (ii) the weight of configurations with charges separated on different fragments (Ω_{CT}) with range from $\Omega_{\mathrm{CT}} = 0$ to $\Omega_{\mathrm{CT}} = 1$, i.e. from localized to pure CT state, and choosing a threshold $\Omega_{\mathrm{CT}} > 0.9$ as indication of a transition of markedly

CT character; and (iii) the electron/hole population on each fragment, close to 0.0/1.0 and 1.0/0.0, respectively, for a pure CT transition.

As a benchmarking case, the metrics computed for the benzene-TCNE example ($\Omega_{\mathrm{POS}} = 1.50$ and $\Omega_{\mathrm{CT}} = 0.98$, for all the double-hybrid methods) perfectly agrees with those calculated from an in-depth analysis of the linear response TD-DFT transition density matrix:[43] a negligible orbital overlap between the frontier molecular orbitals (the $S_1 \leftarrow S_0$ excitation is a $\pi \rightarrow \pi^\star$ transition) and a transfer of a full electron from benzene to TCNE upon excitation. Note that many other descriptors have been proposed in the literature, but we judge that the ones we selected are enough for an unambiguous assignment of the kind of excitation considered. The detailed values of the descriptors are listed for all the systems as supplementary information, and in all cases the criteria are met, thus allowing a statistically consistent and correct analysis. In the case of intra-molecular CT excitations, we split the molecule in two approximately similar fragments according to the structure in terms of donor and acceptor moieties, obtaining now $\Omega_{\mathrm{POS}} \approx 1.5$ but smaller Ω_{CT} values between 0.5–0.7, also in agreement with a partial orbital overlap obtained for e.g. DANS in other works.[43]

3 Results and Discussion

3.1 Intermolecular Charge-Transfer Complexes

3.1.1 Hybrid and Range-Separated Hybrid Functionals

Table 2 gathers the excitation energies computed at the B3LYP, PBE0, M06-2X, and ωB97X levels. We can easily observe, unsurprisingly, a large underestimation of the reference values by these methods, with MSE rang-

ing from –1.54 (B3LYP) to –0.64 eV (M06-2X) increasing with the increase of the value of a_x. On the other hand, the performance of ωB97X is remarkable, with MSE and MUE below 0.1 eV as well as a corresponding RMSE of only 0.06 eV. The maximum deviation (–0.12 eV) was found for the *o*-xylene-TCNE complex. These results agree very well with those previously reported for some of the systems in Ref. 51, using the the def2-TZVP basis set, which also shows the marginal dependence of the results when basis sets as large as a triple-ξ are used. Note how the ω value in the ωB97X model ($\omega = 0.30$) is very close to the optimally tuned value previously found for each of the complexes of the benzene-TCNE, toluene-TCNE, *o*-xylene-TCNE, and naphtalene-TCNE set,[50] in the range $\omega = 0.31 - 0.33$, which helps to explain the remarkable performance of a hybrid range-separated functional as ωB97X is.

We briefly comment on the existence of two reference values for the benzene-TCNE complex in Table 2: a theoretical (3.69 eV) and a gas-phase experimental value (3.59 eV), the latter corresponding to the 2nd excited-state; i.e., the first with a non-vanishing oscillator strength (f), as the 1st excited-state is a dark state. All the theoretical methods considered show a marginal difference between the two excited-states, as little as 0.1 eV, with both states showing a CT character as evidenced by the metrics introduced before. As we did in Ref. 55, we use the latter reference value for the purpose of comparison. However, the reference excitation energy of 3.69 eV calculated at the EOM-CCSD(T) level[43] is also useful to assess previous estimates in literature by sophisticated or more costly *ab initio* methods, and thus to underline more clearly the performance of the methods considered here. Actually, the EOM-CCDS(T) value was overestimated roughly

by 0.3 eV at the EOM-CCSD or CASPT2 levels,[100] showing the intrinsic difficulty to deal with these CT transition by *ab initio* methods. We finally mention other studies of benzene-TCNE and naphtalene-TCNE complexes at the (SCS-)ADC(2) level, and with the MC-PDFT method,[101] also reporting larger errors[102] than those obtained here by ωB97X and range-separated double-hybrid methods (*vide infra*)

3.1.2 Double-Hybrid Functionals

We assess now in detail the performance of B2-PLYP, B2GP-PLYP, PBE0-DH, and PBE-QIDH double-hybrid functionals, using the excitation energies collected in Tables 3 and 4. The MSE values obtained with these methods are still considerably large, showing a systematic underestimation of excitation energies, and are comprised between −1.12 eV (B2-PLYP) and –0.67 eV (PBE-QIDH). The PBE-QIDH values for benzene-TCNE, toluene-TCNE, *o*-xylene-TCNE, and naphtalene-TCNE reasonably agree with those previously computed with the cc-pVDZ basis set,[55] confirming a weak dependence of the results on the basis set being used. To better understand the performance of these double-hybrid methods compared with the hybrid functionals discussed previously, we look at the B2-LYP, B2GP-LYP, PBE0-H, and PBE-QIH values, that is, the excitation energies calculated by hybrid functionals with the same formulation of the double-hybrid ones, i.e. eliminating the third term from Eq. 2 in all cases. We obtain MSE values of –0.59, –0.23, –0.69, and –0.08 eV for B2-LYP, B2GP-LYP, PBE0-H, and PBE-QIH, respectively. Note how the error decreases with increasing the value of a_x as expected from the performance of typical hybrid functionals on these systems, and how the results for PBE0-H or B2-LYP are comparable with that of M06-2X since their a_x values are close. However, since

the contribution of the $a_c\Delta\Omega^{(D)}$ term is always negative for these excitations, the errors (MUE) is increased by 0.53, 0.65, 0.24, and 0.58 eV going from B2-LYP, B2GP-LYP, PBE0-H, and PBE-QIH to the corresponding B2-PLYP, B2GP-PLYP, PBE0-DH, and PBE-QIDH models; again with a strong dependence on the value of a_c. The DSD-PBEP86 functional did not show any significant advantage, with MSE (MUE) of –0.70 (0.70) eV and thus comparable with other double-hybrid models.

3.1.3 Range-Separated Double-Hybrid Functionals

The performance of range-separated double-hybrid functionals (ωB2-PLYP, ωB2GP-PLYP, RSX-0DH, and RSX-QIDH) is considered next using again the results in Tables 3 and 4. Interestingly, all the range-separated models largely outperformed the parent functionals: ωB2-PLYP improves MUE of B2-PLYP by 1.04 eV, ωB2GP-PLYP improves MUE of B2GP-PLYP by 0.73 eV, RSX-0DH improves MUE of PBE0-DH by 0.70 eV, and RSX-QIDH improves MUE of PBE-QIDH by 0.62 eV, in all cases bringing the MUE (or RMSE) mostly below 0.2 eV, which clearly shows the remarkable performance of these methods for such challenging CT transitions. Particularly notable is the accuracy of the RSX-QIDH model, if we consider that its range-separation ω value was not fitted to excited-state energies, but rather chosen to reproduce the energy of the H atom as a physically meaningful limiting case. This leads to the best metric values among the methods considered: as low as MSE = –0.03 eV, MUE = 0.06 eV, RMSE = 0.07 eV, and a maximum deviation of –0.11 eV for the *o*-xylene-TCNE complex. Figure 2 presents the statistical results in a graphical form, to make clear the comparison of the performance of different methods.

We can also consider the results of ωB2-LYP, ωB2GP-LYP, RSX-0H, and RSX-QIH, which are the underlying range-separated hybrid models corresponding to the range-separated double-hybrid functionals, to evaluate separately the effect of the CIS(D)-like correction. Contrarily to non-range-separated models, MSE are always positive, which means a slight and systematic overestimation of the excitation energies by 0.37 eV (ωB2-LYP), 0.44 eV (ωB2GP-LYP), 0.43 eV (RSX-0H), and 0.51 eV (RSX-QIH). Thus, the term $a_c\Delta\Omega^{(D)}$ is responsible for the low errors obtained, showing the delicate interplay of the a_x, a_c, and ω values, which are entirely determined non-empirically in the case of the RSX-0DH and RSX-QIDH functionals.

We are also aware of some previous results applying range-separated double-hybrid models to the benzene-TCNE complex in Ref. 40, in the context of a study of charge-transfer excitations of several systems. Mixing intra- and inter-molecular charge-transfer excitations, with the latter class of excitations only represented by benzene-TCNE, might under-represent the situations where long-range corrections are necessary and thus skew some conclusions about the performance of the methods being considered. As it will be seen below, the errors for intra-molecular excitations might be lower than error due to a skewed representation of long-range effects for inter-molecular charge-transfer excitations. For the benzene-TCNE complex, the B3LYP, ωB97X, B2-PLYP, B2GP-PLYP, ωB2-PLYP, ωB2GP-PLYP, and RSX-QIDH results of Ref. 40 are perfectly reproduced here, within 0.03 eV. However, the results calculated for PBE0-DH, PBE-QIDH, and RSX-0DH deviated by up to 1 eV. More recently, we are also aware of a study [103] including benzene-TCNE, toluene-TCNE, *o*-xylene-TCNE, and naphtalene-TCNE complexes, also updating those data mentioned before, with the results here

in perfect agreement now with them.

3.2 Further benchmarking

3.2.1 Asymptotic Limit of Inter-Molecular Charge-Transfer Excitations

The exploration of the asymptotic limit for charge-transfer excitations, where the weakly interacting molecules are infinitely separated and excitations are thus characterized by an R^{-1} energy decay as a function of the intermolecular separation R, could help to confirm whether the accuracy of the range-separated methods at equilibrium distances ($R = R_e$) is preserved at very large distances ($R \to \infty$). We have chosen the ammonia-fluorine complex, see Figure 3, for which nearly-exact CCSDT-3/cc-pVDZ results are available in both situations (6.62 eV at $R = R_e$ and 10.82 eV at $R \to \infty$) as reference values,[90,104] and checked that the excitation energy at $R \to \infty$ is always characterized by the CT descriptors $\Omega_{\mathrm{POS}} = 1.5$ and $\Omega_{\mathrm{CT}} = 1.0$. We also note the good agreement for the CT descriptors at $R = R_e$ between CC2 and the double-hybrid methods considered here, with $\Omega_{\mathrm{POS}} = 1.47 - 1.49$ and $\Omega_{\mathrm{CT}} = 0.82 - 0.87$ for the latter methods, compared with $\Omega_{\mathrm{POS}} = 1.47$ and $\Omega_{\mathrm{CT}} = 0.86$ at the CC2 level.[90]

Figure 3 depicts the deviation with respect to calculated values, and shows how range-separated double-hybrid functionals slightly but systematically improve the values at $R = R_e$, but do that more significantly at $R \to \infty$, reducing the deviation with respect to the CCSDT-3 reference value by 2–4 eV as compared to standard double-hybrid models. Note also that the range-separated hybrid ωB97X functional gives values of 5.55 and 7.69 eV at $R = R_e$ and $R \to \infty$, respectively, and thus it is not as ac-

curate as the double-hybrid functionals. The DSD-PBEP86 functional, on the other hand, does not improve the results like other double-hybrids, with values of 5.15 and 7.05 eV at $R = R_e$ and $R \to \infty$, respectively. The good performance of the PBE0-DH and PBE-QIDH functionals in both regimes is reasonably accurate as starting point, with the additional improvement that the RSX-based correction bring to both, providing values very close to *ab initio* methods such as CC2 for which an error (with respect to CCSDT-3 values) of 0.65 and 1.14 eV at $R = R_e$ and $R \to \infty$, respectively, was observed before.[90,104]

3.2.2 Potential Energy Curves for Excitation Energies

The description of the whole potential energy curves for the low-lying excited states of the ammonia-fluorine complex will also be considered using PBE-QIDH and RSX-QIDH, which previously provided one of the lowest error out of their families of methods, according to the results presented in Figure 3. That will allow us to explore whether these models also provide a smooth transition from the $R = R_e$ to the $R \to \infty$ regime. Figure 4 shows the evolution of the excited-state energies as a function of the intermolecular separation R. It can be seen how the pronounced dependence of the CT state (indicated as S_2) on the value of R, as well as the progressive crossing of that state with several other curves for the RSX-QIDH case. Actually, the latter seems to behave better than PBE-QIDH for all intermolecular distances, resembling closely the curves obtained using the CC2 method.[104] However, the RSX-QIDH limiting value of the CT state (at $R \to \infty$) still lies below a local excited-state, which is not what it is predicted by CC3 and higher-order methods.[104] The same behavior is expected to be characteristic of other range-separated double-hybrid functionals too, further proving that

there still is some margin of improvement available for these methods.

3.2.3 Intra-Molecular Charge-Transfer Excitations

Intra-molecular charge-transfer excited states are further investigated to confirm whether the remarkable performance of range-separated double-hybrid methods for inter-molecular excitations does also apply to intra-molecular ones. We have selected the push-pull dyes shown in Figure 5 (Coumarin-152, DCS, and DANS dyes) and we collected the results of all methods in Table 5. For this kind of luminophores, the fine-tuning of the ω parameter for range separation[105–107] is known to deliver very accurate values, although at a considerable computational effort and with some geometry dependence.[108] As expected, our results show that B3LYP and PBE0 suffer from large errors, considerably underestimating the reference values, while M06-2X provides values as accurate as those of ωB97X, due to the large EXX component. On the other hand, the double-hybrid methods DSD-PBEP86, B2-PLYP, B2GP-PLYP, PBE0-DH, and PBE-QIDH return smaller errors that hybrids, between 0.06–0.07 eV (DSD-PBEP86 and PBE-QIDH) and 0.11–0.27 eV (B2GP-PLYP, PBE0-DH, and B2-PLYP). The use of a range-separated functional only slightly modifies the results for B2-PLYP; for the B2GP-PLYP, PBE0-DH, and PBE-QIDH models we do not observe an improvement, although still providing an acceptable MUE of 0.3–0.5 eV.

3.2.4 Excitations in Open-Shell Molecular Systems

Finally, we have also selected a set of small radicals as examples of electronic transitions in open-shell molecular systems.[52] Such systems are not routinely studied, and applications of double-hybrid methods are still

scarce.[27] We do not aim to provide a comprehensive benchmarking of TD-DFT methods for these systems, but rather we aim to make a first comparison between hybrid and double-hybrid functionals (see Tables 6 and 7) in view of the nearly-exact reference results that have become available recently.[52] Indeed, Table 6 shows very low MSE for B3LYP, PBE0, and ωB97X methods, but a slightly larger MUE in all cases, indicating some error compensation for these methods. On the other hand, M06-2X systematically underestimates the reference values. The same performance, although slightly reduced, is also found for double-hybrids, providing both low MSE and MUE between 0.03–0.10 and 0.06–0.14 eV, respectively. The use of range-separated double-hybrid functionals does not bring forth any significant change. As an example, B2GP-PLYP provided the lowest errors of all the tested considered, and its extension to ωB2GP-PLYP leads to errors differing by less than 0.01 eV from the B2GP-PLYP ones.

4 Conclusions

We have explored the accuracy of double-hybrid density functionals, in their standard (B2-PLYP, B2GP-PLYP, PBE0-DH, PBE-QIDH) and corresponding range-separated versions (ωB2-PLYP, ωB2GP-PLYP, RSX-0DH, RSX-QIDH), applied to challenging charge-transfer electronic transitions. For this purpose, we selected a set of large and real-world weakly bound complexes, namely benzene-TCNE, toluene-TCNE, *o*-xylene-TCNE, naphtalene-TCNE, hexamethylbenzene-TCNE, diphenylene-TCNE, hexamethylbenzene-chloranil, and diphenylene-chloranil, for which the charge-transfer nature of a low-lying singlet-singlet excitation is clearly established. In addition to charge-transfer excitation energies at equilibrium distances, we

also studied the ammonia-fluorine complex as a benchmark system to follow the excitation energy at infinite separation of the fragments. Furthermore, we also considered a set of push-pull molecules featuring intra-molecular charge-transfer excitations, to cover a wider range of the real-world applications.

The use of range-separation is clearly beneficial for this kind of excitations, be it applied to hybrid or double-hybrid methods, and a viable way to deal with CT transitions independently of the underlying double-hybrid functional being used. We have demonstrated the quality of the ωB2-PLYP, ωB2GP-PLYP, RSX-0DH, and RSX-QIDH models, with ωB2GP-PLYP behaving similarly to ωB2-PLYP, and RSX-QIDH slightly better than RSX-0DH. One could argue that the famous Jacob's Ladder ordering of accuracy is not confirmed in this study, since some of the ωB97X individual errors are comparable or surprisingly lower than those provided by some of the double-hybrid functionals, but that would be a biased argument, since the best range-separated double-hybrid method generally outperforms the corresponding range-separated hybrid functional. Overall, the functionals tend to conform with this approximate hierarchy looking at the whole results of this study, in agreement with previous benchmarking studies.[109] For instance, from a weighted MUE comprising the set of intra- and inter-molecular charge-transfer excitation energies calculated in this work, the error of ωB97X (0.38 eV) is higher than any of the range-separated double-hybrid functionals, from highest to lowest: 0.37, 0.35, 0.34, and 0.25 eV for RSX-0DH, ωB2GP-PLYP, ωB2-PLYP, and RSX-QIDH, respectively.

We have also for the first time assessed whether the quality of double-

hybrid models for CT excitations in the bonding region is also transferred to the asymptotic region, where range-separated double-hybrid models again improve significantly the results. However, such results also underline the need for further improvement which may be achieved with the inclusion of triple excitations in double-hybrid methods, with distance-dependent ω (or μ) values and/or with the inclusion of the extremely long range regime in the training sets used in the parameterization of empirical models. Finally, we would like to point out that the two families of range-separated functionals considered, namely ωB2-PLYP and ωB2GP-PLYP on one hand, RSX-0DH and RSX-QIDH on the other hand, differ in the way in which the optimal value of the range-separation (ω or μ) parameter is set. In the case of the RSX models, ω is not chosen through a fitting of excitation energies, but rather by reproducing the energy of the H atom, with the goal to reduce the self-interaction error, which is a feature of functionals for general-purpose application. Finally, we want to emphasize that reliable exchange-correlation models are a pre-requisite for obtaining accurate results upon range-separation corrections. This is true for both hybrid and double-hybrid models, independently of the expression chosen for that.

Acknowledgements

The work in Alicante is supported by project PID2019-106114GB-I00 ("Ministerio de Ciencia e Innovación"). E.B. thanks ANR (Agence Nationale de la Recherche) and CGI (Commissariat à l'Investissement d'Avenir) for their financial support to this work through Labex SEAM (Science and Engineering for Advanced Materials and devices), Grant Nos. ANR-10-LABX-096 and ANR-18-IDEX-0001. I.C. gratefully acknowledge support

from the European Research Council (ERC) for grant agreement No. 648558 (STRIGES CoG). The authors thank the GENCI-CINES for HPC resources (Project Nos. A0060810359 and A0080810359). We also acknowledge the help of G. Ricci and Y. Olivier (U. Namur, Belgium) with the SCS-CC2 calculations of Coumarin-152, DCS, and DANS dyes.

Supplementary Material

In the Supplementary Material we include: (i) representation of the geometry (orientation) of the weakly bound inter-molecular complexes studied; (ii) numerical values of the metrics used to characterize the inter-molecular CT states of all systems; (iii) calculated excitation energies and CT metrics of the ammonia-fluorine complex at both $R = R_e$ and $R \to \infty$ distances; (iv) sketch of the splitting between donor-acceptor for calculating the metrics for the intra-molecular CT states; and (v) Cartesian (XYZ) atomic coordinates (in Å) of all the systems considered.

References

[1] Zhang, Y.; Xu, X.; Goddard, W. A. Doubly hybrid density functional for accurate descriptions of nonbond interactions, thermochemistry, and thermochemical kinetics. *Proceedings of the National Academy of Sciences* **2009**, *106*, 4963–4968.

[2] Kozuch, S.; Gruzman, D.; Martin, J. M. DSD-BLYP: A general purpose double hybrid density functional including spin component scaling and dispersion correction. *The Journal of Physical Chemistry C* **2010**, *114*, 20801–20808.

[3] Goerigk, L.; Grimme, S. A general database for main group thermo-

chemistry, kinetics, and noncovalent interactions- assessment of common and reparameterized (meta-) GGA density functionals. *Journal of Chemical Theory and Computation* **2010**, *6*, 107–126.

[4] Goerigk, L.; Grimme, S. A thorough benchmark of density functional methods for general main group thermochemistry, kinetics, and noncovalent interactions. *Physical Chemistry Chemical Physics* **2011**, *13*, 6670–6688.

[5] Goerigk, L.; Grimme, S. Efficient and Accurate Double-Hybrid-Meta-GGA Density Functionals Evaluation with the Extended GMTKN30 Database for General Main Group Thermochemistry, Kinetics, and Noncovalent Interactions. *Journal of Chemical Theory and Computation* **2011**, *7*, 291–309.

[6] Zhang, I. Y.; Su, N. Q.; Brémond, E. A.; Adamo, C.; Xu, X. Doubly hybrid density functional xDH-PBE0 from a parameter-free global hybrid model PBE0. *The Journal of Chemical Physics* **2012**, *136*, 174103.

[7] Bousquet, D.; Brémond, E.; Sancho-García, J. C.; Ciofini, I.; Adamo, C. Is there still room for parameter free double hybrids? Performances of PBE0-DH and B2PLYP over extended benchmark Sets. *Journal of Chemical Theory and Computation* **2013**, *9*, 3444–3452.

[8] Kozuch, S.; Martin, J. M. Spin-component-scaled double hybrids: an extensive search for the best fifth-rung functionals blending DFT and perturbation theory. *Journal of Computational Chemistry* **2013**, *34*, 2327–2344.

[9] Su, N. Q.; Yang, W.; Mori-Sanchez, P.; Xu, X. Fractional charge behavior and band gap predictions with the XYG3 type of doubly hybrid

density functionals. *The Journal of Physical Chemistry A* **2014**, *118*, 9201–9211.

[10] Wykes, M.; Su, N. Q.; Xu, X.; Adamo, C.; Sancho-García, J.-C. Double Hybrid Functionals and the Π-System Bond Length Alternation Challenge: Rivaling Accuracy of Post-HF Methods. *Journal of Chemical Theory and Computation* **2015**, *11*, 832–838.

[11] Wykes, M.; Pérez-Jiménez, A.; Adamo, C.; Sancho-García, J.-C. The diene isomerization energies dataset: A difficult test for double-hybrid density functionals? *The Journal of Chemical Physics* **2015**, *142*, 224105.

[12] Brémond, É.; Savarese, M.; Su, N. Q.; Pérez-Jiménez, Á. J.; Xu, X.; Sancho-García, J. C.; Adamo, C. Benchmarking density functionals on structural parameters of small-/medium-sized organic molecules. *Journal of Chemical Theory and Computation* **2016**, *12*, 459–465.

[13] Goerigk, L.; Hansen, A.; Bauer, C.; Ehrlich, S.; Najibi, A.; Grimme, S. A look at the density functional theory zoo with the advanced GMTKN55 database for general main group thermochemistry, kinetics and noncovalent interactions. *Physical Chemistry Chemical Physics* **2017**, *19*, 32184–32215.

[14] Mehta, N.; Casanova-Páez, M.; Goerigk, L. Semi-empirical or non-empirical double-hybrid density functionals: which are more robust? *Physical Chemistry Chemical Physics* **2018**, *20*, 23175–23194.

[15] Goerigk, L.; Mehta, N. A trip to the density functional theory zoo: warnings and recommendations for the user. *Australian Journal of Chemistry* **2019**, *72*, 563–573.

[16] Lonsdale, D. R.; Goerigk, L. The one-electron self-interaction error in 74 density functional approximations: a case study on hydrogenic mono-and dinuclear systems. *Physical Chemistry Chemical Physics* **2020**, *22*, 15805–15830.

[17] Martin, J. M.; Santra, G. Empirical Double-Hybrid Density Functional Theory: A 'Third Way' in Between WFT and DFT. *Israel Journal of Chemistry* **2020**, *60*, 787–804.

[18] Savarese, M.; Brémond, E.; Ciofini, I.; Adamo, C. Electron Spin Densities and Density Functional Approximations: Open-Shell Polycyclic Aromatic Hydrocarbons as case study. *Journal of Chemical Theory and Computation* **2020**, *16*, 3567–3577.

[19] Brémond, E.; Savarese, M.; Pérez-Jiménez, Á. J.; Sancho-García, J. C.; Adamo, C. Systematic improvement of density functionals through parameter-free hybridization schemes. *The Journal of Physical Chemistry Letters* **2015**, *6*, 3540–3545.

[20] Goerigk, L.; Moellmann, J.; Grimme, S. Computation of accurate excitation energies for large organic molecules with double-hybrid density functionals. *Physical Chemistry Chemical Physics* **2009**, *11*, 4611–4620.

[21] Goerigk, L.; Grimme, S. Assessment of TD-DFT methods and of various spin scaled CIS(D) and CC2 versions for the treatment of low-lying valence excitations of large organic dyes. *The Journal of Chemical Physics* **2010**, *132*, 184103.

[22] Goerigk, L.; Grimme, S. Double-hybrid density functionals provide a balanced description of excited ^1L_a and ^1L_b states in polycyclic aro-

matic hydrocarbons. *Journal of Chemical Theory and Computation* **2011**, *7*, 3272–3277.

[23] Meo, F. D.; Trouillas, P.; Adamo, C.; Sancho-García, J.-C. Application of recent double-hybrid density functionals to low-lying singlet-singlet excitation energies of large organic compounds. *The Journal of Chemical Physics* **2013**, *139*, 164104.

[24] Sancho-García, J.-C.; Adamo, C.; Pérez-Jiménez, A. Describing excited states of [n]cycloparaphenylenes by hybrid and double-hybrid density functionals: from isolated to weakly interacting molecules. *Theoretical Chemistry Accounts* **2016**, *135*, 25.

[25] Alipour, M. On the performance of time-dependent double-hybrid density functionals for description of absorption and emission spectra of heteroaromatic compounds. *Theoretical Chemistry Accounts* **2016**, *135*, 67.

[26] Brémond, É.; Savarese, M.; Pérez-Jiménez, Á. J.; Sancho-García, J. C.; Adamo, C. Speed-up of the excited-state benchmarking: Double-hybrid density functionals as test cases. *Journal of Chemical Theory and Computation* **2017**, *13*, 5539–5551.

[27] Hernández-Martínez, L.; Brémond, E.; Pérez-Jiménez, A. J.; San-Fabián, E.; Adamo, C.; Sancho-García, J. C. Nonempirical (double-hybrid) density functionals applied to atomic excitation energies: A systematic basis set investigation. *International Journal of Quantum Chemistry* **2020**, *120*, e26193.

[28] Goerigk, L.; Casanova-Paéz, M. The Trip to the Density Functional Theory Zoo Continues: Making a Case for Time-Dependent Double

Hybrids for Excited-State Problems. *Australian Journal of Chemistry* **2020**, *74*, 3–15.

[29] Chan, B.; Goerigk, L.; Radom, L. On the inclusion of post-MP2 contributions to double-Hybrid density functionals. *Journal of Computational Chemistry* **2016**, *37*, 183–193.

[30] Schwabe, T.; Goerigk, L. Time-dependent double-hybrid density functionals with spin-component and spin-opposite scaling. *Journal of Chemical Theory and Computation* **2017**, *13*, 4307–4323.

[31] Tozer, D.; Handy, N. On the determination of excitation energies using density functional theory. *Physical Chemistry Chemical Physics* **2000**, *2*, 2117–2121.

[32] Tozer, D. Relationship between long-range charge-transfer excitation energy error and integer discontinuity in KohnSham theory. *The Journal of Chemical Physics* **2003**, *119*, 12697–12699.

[33] Peach, M. J.; Benfield, P.; Helgaker, T.; Tozer, D. J. Excitation energies in density functional theory: An evaluation and a diagnostic test. *The Journal of Chemical Physics* **2008**, *128*, 044118.

[34] Zhang, I. Y.; Xu, X. Reaching a uniform accuracy for complex molecular systems: long-range-corrected XYG3 doubly hybrid density functional. *The Journal of Physical Chemistry Letters* **2013**, *4*, 1669–1675.

[35] Mardirossian, N.; Head-Gordon, M. Survival of the most transferable at the top of Jacobs ladder: Defining and testing the ω B97M(2) double hybrid density functional. *The Journal of Chemical Physics* **2018**, *148*, 241736.

[36] Brémond, E.; Savarese, M.; Pérez-Jiménez, Á. J.; Sancho-García, J. C.; Adamo, C. Range-Separated Double-Hybrid Functional from Nonempirical Constraints. *Journal of Chemical Theory and Computation* **2018**, *14*, 4052–4062.

[37] Brémond, É.; Pérez-Jiménez, Á. J.; Sancho-García, J. C.; Adamo, C. Range-separated hybrid density functionals made simple. *The Journal of Chemical Physics* **2019**, *150*, 201102.

[38] Brémond, É.; Pérez-Jiménez, Á. J.; Sancho-García, J. C.; Adamo, C. Range-separated hybrid and double-hybrid density functionals: A quest for the determination of the range-separation parameter. *The Journal of Chemical Physics* **2020**, *152*, 244124.

[39] Casanova-Páez, M.; Dardis, M. B.; Goerigk, L. ωB2PLYP and ωB2GPPLYP: the first two double-hybrid density functionals with long-range correction optimized for excitation energies. *Journal of Chemical Theory and Computation* **2019**, *15*, 4735–4744.

[40] Casanova-Páez, M.; Goerigk, L. Assessing the Tamm–Dancoff approximation, singlet–singlet, and singlet–triplet excitations with the latest long-range corrected double-hybrid density functionals. *The Journal of Chemical Physics* **2020**, *153*, 064106.

[41] Hirata, S.; Head-Gordon, M. Time-dependent density functional theory within the Tamm–Dancoff approximation. *Chemical Physics Letters* **1999**, *314*, 291–299.

[42] Dreuw, A.; Weisman, J. L.; Head-Gordon, M. Long-range charge-transfer excited states in time-dependent density functional theory require non-local exchange. *The Journal of Chemical Physics* **2003**, *119*, 2943–2946.

[43] Moore, B.; Sun, H.; Govind, N.; Kowalski, K.; Autschbach, J. Charge-Transfer Versus Charge-Transfer-Like Excitations Revisited. *Journal of Chemical Theory and Computation* **2015**, *11*, 3305–3320.

[44] Cornil, J.; Verlaak, S.; Martinelli, N.; Mityashin, A.; Olivier, Y.; Van Regemorter, T.; D'Avino, G.; Muccioli, L.; Zannoni, C.; Castet, F.; Beljonne, D.; Heremans, P. Exploring the energy landscape of the charge transport levels in organic semiconductors at the molecular scale. *Accounts of Chemical Research* **2013**, *46*, 434–443.

[45] Coropceanu, V.; Chen, X.-K.; Wang, T.; Zheng, Z.; Brédas, J.-L. Charge-transfer electronic states in organic solar cells. *Nature Reviews Materials* **2019**, *4*, 689–707.

[46] Khan, S.-U.-Z.; Londi, G.; Liu, X.; Fusella, M. A.; D'Avino, G.; Muccioli, L.; Brigeman, A. N.; Niesen, B.; Yang, T. C.-J.; Olivier, Y.; Dull, J.; Giebink, N.; Beljonne, D.; Rand, B. Multiple Charge Transfer States in Donor–Acceptor Heterojunctions with Large Frontier Orbital Energy Offsets. *Chemistry of Materials* **2019**, *31*, 6808–6817.

[47] Santoro, F.; Barone, V.; Improta, R. Can TD-DFT calculations accurately describe the excited states behavior of stacked nucleobases? The cytosine dimer as a test case. *Journal of Computational Chemistry* **2008**, *29*, 957–964.

[48] Improta, R.; Barone, V. Interplay between "Neutral" and "Charge-Transfer" Excimers Rules the Excited State Decay in Adenine-Rich Polynucleotides. *Angewandte Chemie International Edition* **2011**, *50*, 12016–12019.

[49] Huix-Rotllant, M.; Brazard, J.; Improta, R.; Burghardt, I.; Markovitsi, D. Stabilization of mixed Frenkel-charge transfer excitons

extended across both strands of guanine–cytosine DNA duplexes. *The Journal of Physical Chemistry Letters* **2015**, *6*, 2247–2251.

[50] Stein, T.; Kronik, L.; Baer, R. Reliable prediction of charge transfer excitations in molecular complexes using time-dependent density functional theory. *Journal of the American Chemical Society* **2009**, *131*, 2818–2820.

[51] Ristaus, T.; Hansen, A.; Grimme, S. Excited states using the simplified TammDancoff-Approach for range-separated hybrid density functionals: development and application. *Physical Chemistry Chemical Physics* **2014**, *16*, 14408.

[52] Loos, P.-F.; Lipparini, F.; Boggio-Pasqua, M.; Scemama, A.; Jacquemin, D. A Mountaineering Strategy to Excited States: Highly Accurate Energies and Benchmarks for Medium Sized Molecules. *Journal of Chemical Theory and Computation* **2020**, *16*, 1711–1741.

[53] Ai, X.; Evans, E. W.; Dong, S.; Gillett, A. J.; Guo, H.; Chen, Y.; Hele, T. J.; Friend, R. H.; Li, F. Efficient radical-based light-emitting diodes with doublet emission. *Nature* **2018**, *563*, 536–540.

[54] Guo, H.; Peng, Q.; Chen, X.-K.; Gu, Q.; Dong, S.; Evans, E. W.; Gillett, A. J.; Ai, X.; Zhang, M.; Credgington, D.; Coropceanu, V.; Friend, R. H.; Brédas, J.-L.; Li, F. High stability and luminescence efficiency in donor–acceptor neutral radicals not following the Aufbau principle. *Nature Materials* **2019**, *18*, 977–984.

[55] Ottochian, A.; Morgillo, C.; Ciofini, I.; Frisch, M. J.; Scalmani, G.; Adamo, C. Double hybrids and time-dependent density functional theory: An implementation and benchmark on charge transfer excited states. *Journal of Computational Chemistry* **2020**, *41*, 1242–1251.

[56] Förster, A.; Visscher, L. Double hybrid DFT calculations with Slater type orbitals. *Journal of Computational Chemistry* **2020**, *41*, 1660–1684.

[57] Schwabe, T.; Grimme, S. Theoretical thermodynamics for large molecules: walking the thin line between accuracy and computational cost. *Accounts of Chemical Research* **2008**, *41*, 569–579.

[58] Grimme, S. Density functional theory with London dispersion corrections. *Wiley Interdisciplinary Reviews: Computational Molecular Science* **2011**, *1*, 211–228.

[59] Sancho-García, J.-C.; Adamo, C. Double-hybrid density functionals: merging wavefunction and density approaches to get the best of both worlds. *Physical Chemistry Chemical Physics* **2013**, *15*, 14581–14594.

[60] Goerigk, L.; Grimme, S. Double-hybrid density functionals. *Wiley Interdisciplinary Reviews: Computational Molecular Science* **2014**, *4*, 576–600.

[61] Brémond, E.; Ciofini, I.; Sancho-García, J. C.; Adamo, C. Nonempirical double-hybrid functionals: An effective tool for chemists. *Accounts of chemical research* **2016**, *49*, 1503–1513.

[62] Grimme, S. Semiempirical hybrid density functional with perturbative second-order correlation. *The Journal of Chemical Physics* **2006**, *124*, 034108.

[63] Karton, A.; Tarnopolsky, A.; Lamére, J.-F.; Schatz, G. C.; Martin, J. M. Highly accurate first-principles benchmark data sets for the parametrization and validation of density functional and other approximate methods. Derivation of a robust, generally applicable, double-

hybrid functional for thermochemistry and thermochemical kinetics. *The Journal of Physical Chemistry A* **2008**, *112*, 12868–12886.

[64] Brémond, E.; Adamo, C. Seeking for parameter-free double-hybrid functionals: the PBE0-DH model. *The Journal of Chemical Physics* **2011**, *135*, 024106.

[65] Brémond, É.; Sancho-García, J.; Pérez-Jiménez, Á.; Adamo, C. Communication: double-hybrid functionals from adiabatic-connection: the QIDH model. *The Journal of Chemical Physics* **2014**, *141*, 031101.

[66] Kozuch, S.; Martin, J. M. DSD-PBEP86: in search of the best double-hybrid DFT with spin-component scaled MP2 and dispersion corrections. *Physical Chemistry Chemical Physics* **2011**, *13*, 20104–20107.

[67] Santra, G.; Sylvetsky, N.; Martin, J. M. Minimally empirical double-hybrid functionals trained against the GMTKN55 database: revDSD-PBEP86-D4, revDOD-PBE-D4, and DOD-SCAN-D4. *The Journal of Physical Chemistry A* **2019**, *123*, 5129–5143.

[68] Grimme, S.; Goerigk, L.; Fink, R. F. Spin-component-scaled electron correlation methods. *Wiley Interdisciplinary Reviews: Computational Molecular Science* **2012**, *2*, 886–906.

[69] Brémond, É.; Savarese, M.; Sancho-García, J. C.; Pérez-Jiménez, Á. J.; Adamo, C. Quadratic integrand double-hybrid made spin-component-scaled. *The Journal of Chemical Physics* **2016**, *144*, 124104.

[70] Becke, A. D. Density-Functional Thermochemistry. III. The Role of Exact Exchange. *The Journal of Chemical Physics* **1993**, *98*, 5648–5652.

[71] Adamo, C.; Barone, V. Toward reliable density functional methods without adjustable parameters: The PBE0 model. *The Journal of Chemical Physics* **1999**, *110*, 6158–6170.

[72] Zhao, Y.; Truhlar, D. G. The M06 suite of density functionals for main group thermochemistry, thermochemical kinetics, noncovalent interactions, excited states, and transition elements: two new functionals and systematic testing of four M06-class functionals and 12 other functionals. *Theoretical Chemistry Accounts* **2008**, *120*, 215–241.

[73] Chai, J.-D.; Head-Gordon, M. Systematic optimization of long-range corrected hybrid density functionals. *The Journal of Chemical Physics* **2008**, *128*, 084106.

[74] Grimme, S.; Neese, F. Double-hybrid density functional theory for excited electronic states of molecules. *The Journal of Chemical Physics* **2007**, *127*, 154116.

[75] Head-Gordon, M.; Rico, R. J.; Oumi, M.; Lee, T. J. A doubles correction to electronic excited states from configuration interaction in the space of single substitutions. *Chemical Physics Letters* **1994**, *219*, 21–29.

[76] Perdew, J. P.; Burke, K.; Ernzerhof, M. Generalized gradient approximation made simple. *Physical Review Letters* **1996**, *77*, 3865.

[77] Becke, A. D. Density-functional exchange-energy approximation with correct asymptotic behavior. *Physical Review A* **1988**, *38*, 3098.

[78] Lee, C.; Yang, W.; Parr, R. G. Development of the Colle-Salvetti correlation-energy formula into a functional of the electron density. *Physical Review B* **1988**, *37*, 785.

[79] Kendall, R. A.; Dunning Jr, T. H.; Harrison, R. J. Electron affinities of the first-row atoms revisited. Systematic basis sets and wave functions. *The Journal of Chemical Physics* **1992**, *96*, 6796–6806.

[80] Frisch, M. J. et al. Gaussian16 Revision J.02. 2016; Gaussian Inc. Wallingford CT.

[81] Neese, F. The ORCA program system. *Wiley Interdisciplinary Reviews: Computational Molecular Science* **2012**, *2*, 73–78.

[82] Neese, F. Software update: the ORCA program system, version 4.0. *Wiley Interdisciplinary Reviews: Computational Molecular Science* **2018**, *8*, e1327.

[83] Neese, F.; Wennmohs, F.; Hansen, A.; Becker, U. Efficient, approximate and parallel Hartree–Fock and hybrid DFT calculations. A chain-of-spheres algorithm for the Hartree–Fock exchange. *Chemical Physics* **2009**, *356*, 98–109.

[84] Stoychev, G. L.; Auer, A. A.; Neese, F. Automatic generation of auxiliary basis sets. *Journal of Chemical Theory and Computation* **2017**, *13*, 554–562.

[85] Masnovi, J.; Seddon, E.; Kochi, J. Electron transfer from anthracenes. Comparison of photoionization, charge-transfer excitation and electrochemical oxidation. *Canadian Journal of Chemistry* **1984**, *62*, 2552–2559.

[86] Christiansen, O.; Koch, H.; Jørgensen, P. The second-order approximate coupled cluster singles and doubles model CC2. *Chemical Physics Letters* **1995**, *243*, 409–418.

[87] Hellweg, A.; Grün, S. A.; Hättig, C. Benchmarking the performance of spin-component scaled CC2 in ground and electronically excited states. *Physical Chemistry Chemical Physics* **2008**, *10*, 4119–4127.

[88] Suellen, C.; Freitas, R. G.; Loos, P.-F.; Jacquemin, D. Cross-comparisons between experiment, TD-DFT, CC, and ADC for transition energies. *Journal of Chemical Theory and Computation* **2019**, *15*, 4581–4590.

[89] Loos, P.-F.; Scemama, A.; Jacquemin, D. The Quest For Highly Accurate Excitation Energies: A Computational Perspective. *The Journal of Physical Chemistry Letters* **2020**, *11*, 2374–2383.

[90] Kozma, B.; Tajti, A.; Demoulin, B.; Izsák, R.; Nooijen, M.; Szalay, P. G. A New Benchmark Set for Excitation Energy of Charge Transfer States: Systematic Investigation of Coupled-Cluster Type Methods. *Journal of Chemical Theory and Computation* **2020**, *16*, 4213–4225.

[91] Campetella, M.; Maschietto, F.; Frisch, M. J.; Scalmani, G.; Ciofini, I.; Adamo, C. Charge transfer excitations in TDDFT: A ghost-hunter index. *Journal of Computational Chemistry* **2017**, *38*, 2151–2156.

[92] Savarese, M.; Guido, C. A.; Brémond, E.; Ciofini, I.; Adamo, C. Metrics for molecular electronic excitations: A comparison between orbital-and density-based descriptors. *The Journal of Physical Chemistry A* **2017**, *121*, 7543–7549.

[93] Plasser, F. TheoDORE: A toolbox for a detailed and automated analysis of electronic excited state computations. *The Journal of Chemical Physics* **2020**, *152*, 084108.

[94] Kimber, P.; Plasser, F. Toward an understanding of electronic excitation energies beyond the molecular orbital picture. *Physical Chemistry Chemical Physics* **2020**, *22*, 6058–6080.

[95] Plasser, F.; Lischka, H. Analysis of excitonic and charge transfer interactions from quantum chemical calculations. *Journal of Chemical Theory and Computation* **2012**, *8*, 2777–2789.

[96] Plasser, F.; Wormit, M.; Dreuw, A. New tools for the systematic analysis and visualization of electronic excitations. I. Formalism. *The Journal of Chemical Physics* **2014**, *141*, 024106.

[97] Bäppler, S. A.; Plasser, F.; Wormit, M.; Dreuw, A. Exciton analysis of many-body wave functions: Bridging the gap between the quasiparticle and molecular orbital pictures. *Physical Review A* **2014**, *90*, 052521.

[98] Mewes, S. A.; Mewes, J.-M.; Dreuw, A.; Plasser, F. Excitons in poly (para phenylene vinylene): A quantum-chemical perspective based on high-level ab initio calculations. *Physical Chemistry Chemical Physics* **2016**, *18*, 2548–2563.

[99] Plasser, F. Entanglement entropy of electronic excitations. *The Journal of Chemical Physics* **2016**, *144*, 194107.

[100] Jacquemin, D.; Duchemin, I.; Blase, X. Is the Bethe–Salpeter formalism accurate for excitation energies? Comparisons with TD-DFT, CASPT2, and EOM-CCSD. *The Journal of Physical Chemistry Letters* **2017**, *8*, 1524–1529.

[101] Pandharkar, R.; Hermes, M. R.; Truhlar, D. G.; Gagliardi, L. A New Mixing of Nonlocal Exchange and Nonlocal Correlation with Multi-

configuration Pair-Density Functional Theory. *The Journal of Physical Chemistry Letters* **2020**, *11*, 10158–10163.

[102] Aquino, A. A.; Borges, I.; Nieman, R.; Köhn, A.; Lischka, H. Intermolecular interactions and charge transfer transitions in aromatic hydrocarbon–tetracyanoethylene complexes. *Physical Chemistry Chemical Physics* **2014**, *16*, 20586–20597.

[103] Casanova-Páez, M.; Goerigk, L. Global double hybrids do not work for charge transfer: A comment on Double hybrids and time-dependent density functional theory: An implementation and benchmark on charge transfer excited states. *Journal of Computational Chemistry* **2021**, DOI: 10.1002/jcc.26478.

[104] Kozma, B.; Berraud-Pache, R.; Tajti, A.; Szalay, P. G. Potential energy surfaces of Charge Transfer states. *Molecular Physics* **2020**, *118*, e1776903.

[105] Sun, H.; Zhong, C.; Brédas, J.-L. Reliable prediction with tuned range-separated functionals of the singlet–triplet gap in organic emitters for thermally activated delayed fluorescence. *Journal of Chemical Theory and Computation* **2015**, *11*, 3851–3858.

[106] Penfold, T. J. On predicting the excited-state properties of thermally activated delayed fluorescence emitters. *The Journal of Physical Chemistry C* **2015**, *119*, 13535–13544.

[107] Manna, D.; Blumberger, J.; Martin, J. M.; Kronik, L. Prediction of electronic couplings for molecular charge transfer using optimally tuned range-separated hybrid functionals. *Molecular Physics* **2018**, *116*, 2497–2505.

[108] Eng, J.; Laidlaw, B. A.; Penfold, T. J. On the geometry dependence of tuned-range separated hybrid functionals. *Journal of Computational Chemistry* **2019**, *40*, 2191–2199.

[109] Mardirossian, N.; Head-Gordon, M. Thirty years of density functional theory in computational chemistry: an overview and extensive assessment of 200 density functionals. *Molecular Physics* **2017**, *115*, 2315–2372.

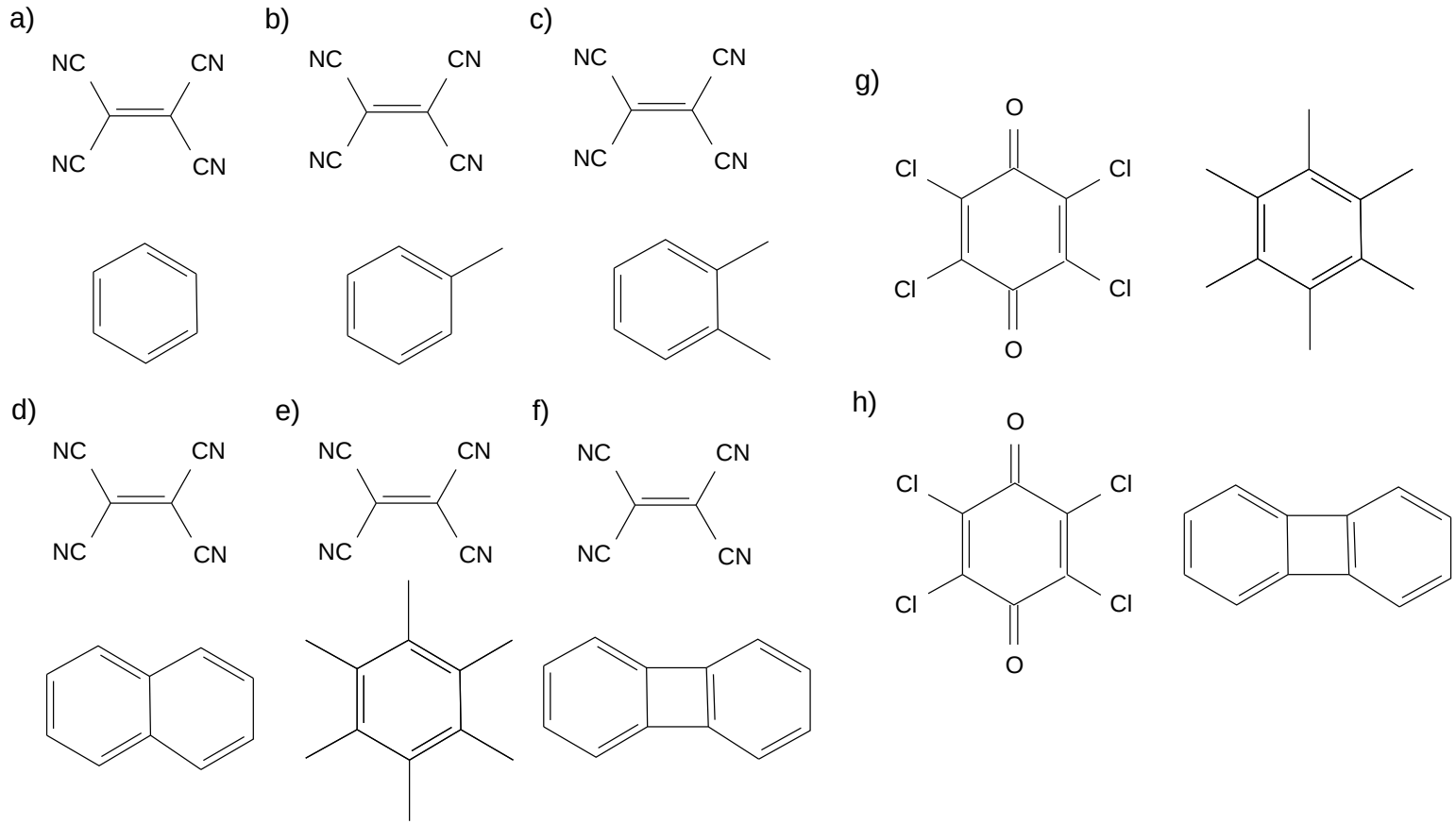

Figure 1: Chemical structure of the weakly interacting dimers studied: a) benzene-TCNE, b) toluene-TCNE, c) *o*-xylene-TCNE, d) naphtalene-TCNE, e) hexamethylbenzene-TCNE, f) diphenylene-TCNE, g) hexamethylbenzene-chloranil, and h) diphenylene-chloranil.

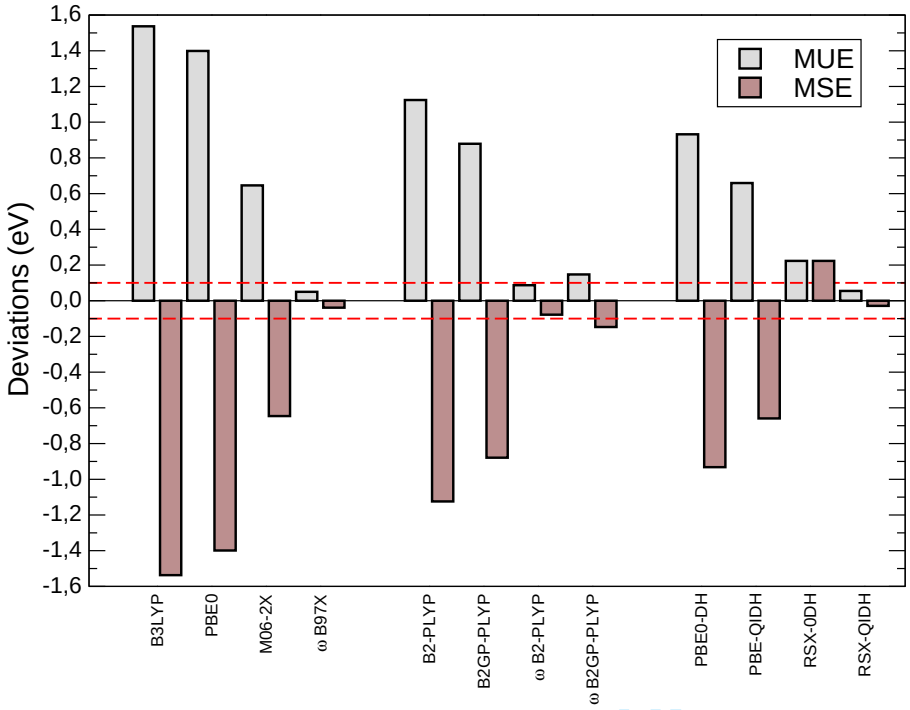

Figure 2: Deviations for each method, with respect to reference values, for the excitation energies of the set of weakly interacting dimers considered. The dashed red lines represent a deviation of ± 0.1 eV with respect to reference results. All calculation use the cc-pVTZ basis set.

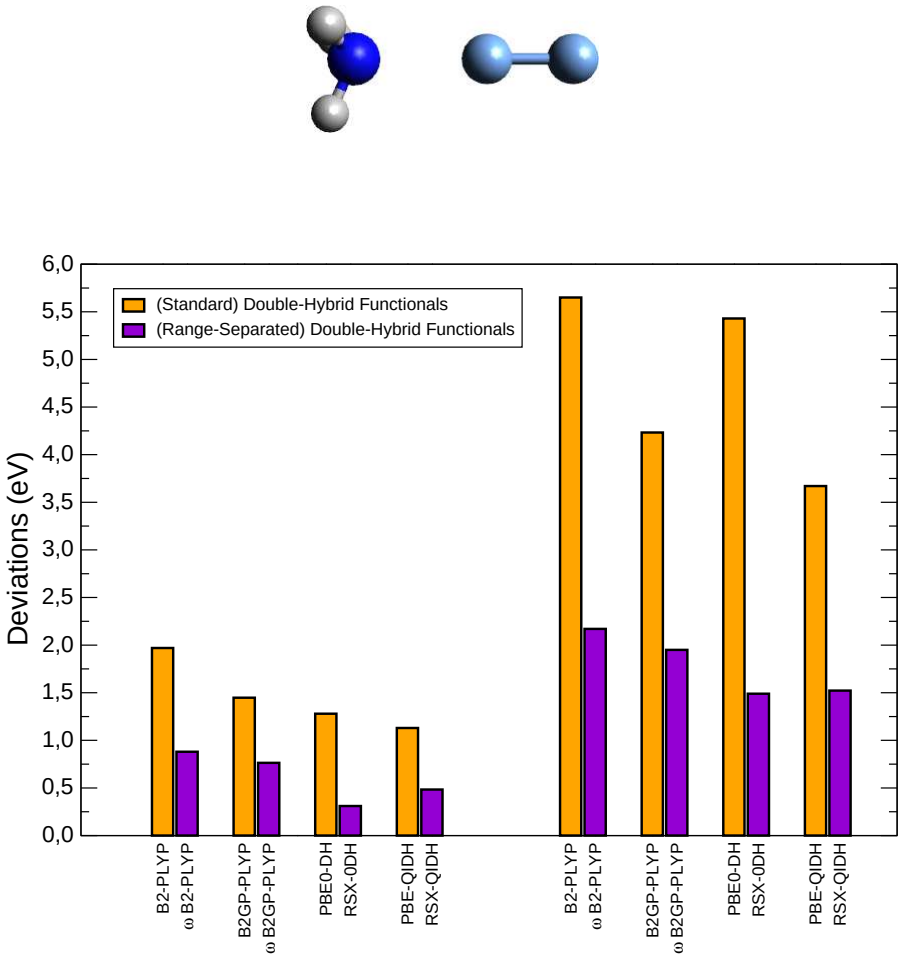

Figure 3: Deviations for each method, with respect to CCSDT-3 reference values, for the excitation energies at the equilibrium ($R = R_e$) and infinite ($R = \infty$) separation of the ammonia-fluorine complex. The first group of values refer to $R = R_e$ (left) and the second to $R \to \infty$ (right). All calculations use the cc-pVDZ basis set.

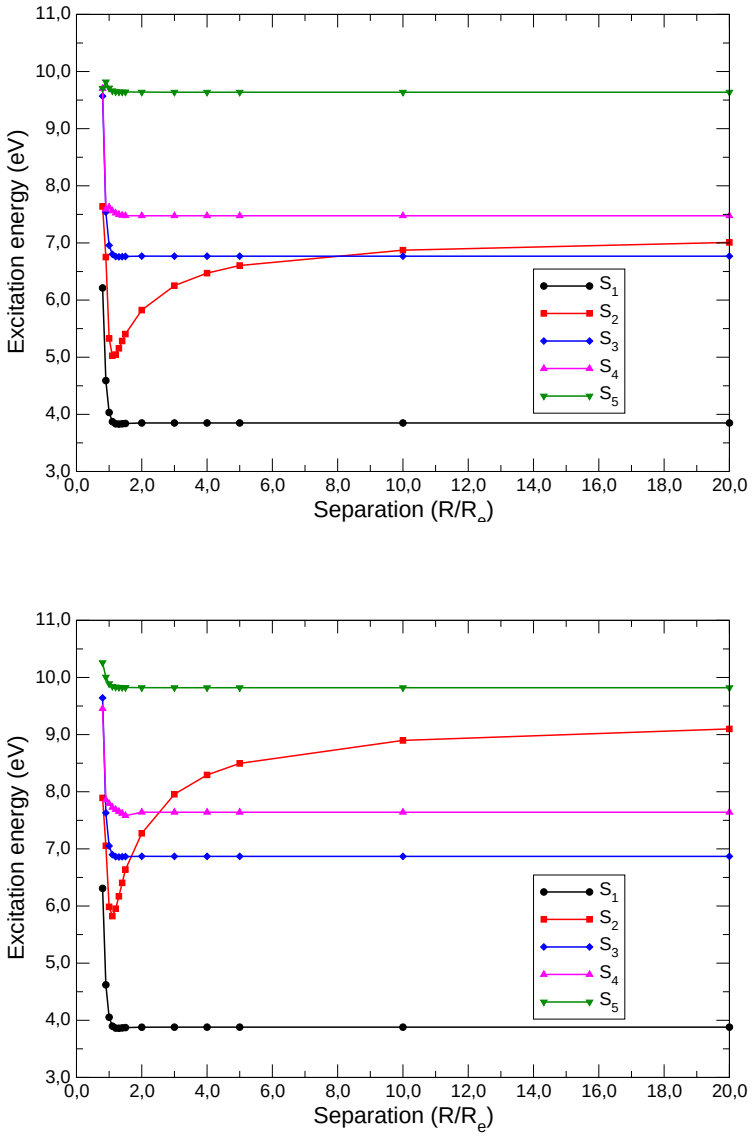

Figure 4: Evolution of the energy of the lowest excited states of the ammonia-fluorine complex, as a function of the intermolecular separation, for PBE-QIDH (top) and RSX-QIDH (bottom) using the cc-pVTZ basis set.

a)

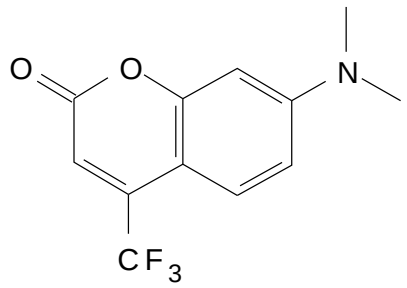

b)

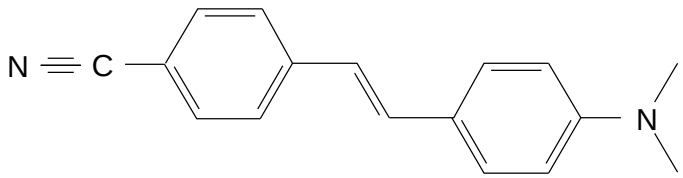

c)

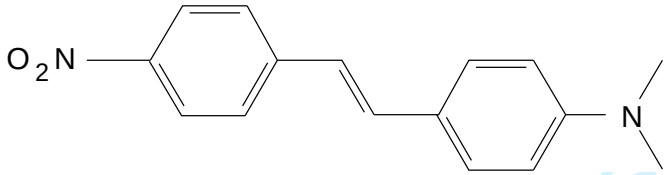

Figure 5: Chemical structure of the molecules: a) coumarin-152, b) DCS, and c) DANS.

Table 1: Values of the coefficients of the EXX and PT2 terms, as well as the range-separation parameter (bohr^{-1})

Functional	a_x	a_c	ω
DSD-PBEP86	0.69	0.52/0.22[a]	
B2-PLYP	0.53	0.27	–
B2GP-PLYP	0.65	0.36	–
ωB2-PLYP	0.53	0.27	0.30
ωB2GP-PLYP	0.65	0.36	0.27
PBE0-DH	1/2	$1/2^3$	–
PBE-QIDH	$3^{-1/3}$	1/3	–
RSX-0DH	1/2	$1/2^3$	0.33
RSX-QIDH	$3^{-1/3}$	1/3	0.27

[a] The specific formulation of the correlation term in DSD-PBEP86 equals $(1 - a_c) = 0.44$, but includes a scaling of same- (0.52) and opposite-spin (0.22) contributions to the PT2 energy.

Table 2: Calculated excitation energies (in eV) for the weakly bound complexes considered, displaying inter-molecular CT excitations, for global and range-separated hybrid functionals using the cc-pVTZ basis set.

Compound	B3LYP	PBE0	M06-2X	ωB97X	Reference
benzene-TCNE	1.989	2.157	2.976	3.612	3.69[a], 3.59[b]
toluene-TCNE	1.743	1.888	2.670	3.275	3.36[b]
o-xylene-TCNE	1.479	1.628	2.420	3.027	3.15[b]
naphtalene-TCNE	0.811	1.000	1.856	2.587	2.60[b]
hexamethylbenzene-TCNE	1.087	1.190	1.828	2.332	2.36[c]
diphenylene-TCNE	0.822	0.914	1.573	2.200	2.28[c]
hexamethylbenzene-chloranil	1.304	1.450	2.291	2.854	2.87[c]
diphenylene-chloranil	1.497	1.611	2.308	2.836	2.81[c]
MSE	–1.54	–1.40	–0.64	–0.04	
MUE	1.54	1.40	0.64	0.05	
MAX	–1.79	–1.60	–0.74	–0.12	

[a] EOM-CCSD(T)/TZVP, taken from Ref. 43.
[b] Gas-phase experimental values, taken from Ref. 85.
[c] SCS-CC2/def2-TZVP(-f), taken from Ref. 51.

Table 3: Calculated excitation energies (in eV) for the weakly bound complexes considered, displaying inter-molecular CT excitations, for global and range-separated double-hybrid functionals using the cc-pVTZ basis set.

Compound	DSD-PBEP86	B2-PLYP	B2GP-PLYP	ωB2-PLYP	ωB2GP-PLYP	Reference
benzene-TCNE	2.991	2.550	2.824	3.614	3.557	3.69[a], 3.59[b]
toluene-TCNE	2.648	2.230	2.485	3.258	3.200	3.36[b]
o-xylene-TCNE	2.389	1.969	2.222	2.995	2.934	3.15[b]
naphtalene-TCNE	1.909	1.427	1.697	2.543	2.475	2.60[b]
hexamethylbenzene-TCNE	1.646	1.300	1.505	2.244	2.170	2.36[c]
diphenylene-TCNE	1.529	1.107	1.338	2.140	2.065	2.28[c]
hexamethylbenzene-chloranil	2.173	1.722	1.983	2.827	2.764	2.87[c]
diphenylene-chloranil	2.154	1.753	1.966	2.774	2.691	2.81[c]
MSE	–0.70	–1.12	–0.88	–0.08	–0.15	
MUE	0.70	1.12	0.88	0.08	0.15	
MAX	–0.76	–1.18	–0.94	–0.16	–0.22	

[a] EOM-CCSD(T)/TZVP, taken from Ref. 43.
[b] Gas-phase experimental values, taken from Ref. 85.
[c] SCS-CC2/def2-TZVP(-f), taken from Ref. 51.

Table 4: Calculated excitation energies (in eV) for the weakly bound complexes considered, displaying inter-molecular CT excitations, for global and range-separated double-hybrid functionals using the cc-pVTZ basis set.

Compound	PBE0-DH	PBE-QIDH	RSX-0DH	RSX-QIDH	Reference
benzene-TCNE	2.719	3.024	3.897	3.670	3.69[a], 3.59[b]
toluene-TCNE	2.403	2.679	3.541	3.310	3.36[b]
o-xylene-TCNE	2.143	2.415	3.283	3.044	3.15[b]
naphtalene-TCNE	1.589	1.904	2.840	2.594	2.60[b]
hexamethylbenzene-TCNE	1.522	1.694	2.554	2.283	2.36[c]
diphenylene-TCNE	1.296	1.537	2.439	2.182	2.28[c]
hexamethylbenzene-chloranil	1.956	2.203	3.151	2.887	2.87[c]
diphenylene-chloranil	1.987	2.174	3.102	2.815	2.81[c]
MSE	–0.93	–0.67	0.22	–0.03	
MUE	0.93	0.67	0.22	0.06	
MAX	–1.02	–0.74	0.29	–0.11	

[a] EOM-CCSD(T)/TZVP, taken from Ref. 43.
[b] Gas-phase experimental values, taken from Ref. 85.
[c] SCS-CC2/def2-TZVP(-f), taken from Ref. 51.

Table 5: Calculated excitation energies (in eV) for the molecules considered, displaying intra-molecular CT excitations, for global and range-separated hybrid and double-hybrid functionals using the cc-pVTZ basis set.

Method	Coumarin-152	DCS	DANS	MSE	MUE	MAX
B3LYP	3.399	3.074	2.658	–0.54	0.54	–0.79
PBE0	3.502	3.166	2.800	–0.43	0.43	–0.65
M06-2X	3.789	3.460	3.254	–0.09	0.13	–0.20
ωB97X	3.955	3.668	3.539	0.13	0.13	0.23
DSD-PBEP86	3.722	3.544	3.302	–0.06	0.06	–0.15
B2-PLYP	3.579	3.352	3.031	–0.27	0.27	–0.42
B2GP-PLYP	3.713	3.498	3.230	–0.11	0.11	–0.22
ωB2-PLYP	4.055	3.799	3.638	0.24	0.24	0.33
ωB2GP-PLYP	4.027	3.790	3.621	0.23	0.23	0.30
PBE0-DH	3.821	3.498	3.209	–0.08	0.14	–0.24
PBE-QIDH	3.845	3.597	3.360	0.01	0.07	0.12
RSX-0DH	4.245	3.914	3.771	0.39	0.39	0.52
RSX-QIDH	4.101	3.839	3.678	0.29	0.29	0.38
Reference	3.723[a]	3.587[a]	3.450[a]			

[a] SCS-CC2/cc-pVTZ values calculated in this work.

Table 6: Calculated excitation energies (in eV) for the radical systems considered, for global and range-separated hybrid functionals using the aug-cc-pVTZ basis set.

Compound	State	B3LYP	PBE0	M06-2X	ωB97X	Reference[a]
BH_2	$^2B_1$	1.310	1.305	0.574	1.300	1.18
HCO	$^2A''$	2.214	2.202	1.730	2.185	2.09
	$^2A'$	4.998	5.185	5.303	5.593	5.45
HOC	$^2A''$	1.057	1.046	0.494	1.009	0.92
H_2PO	$^2A''$	2.652	2.775	2.299	2.752	2.80
	$^2A'$	4.136	4.142	3.861	4.173	4.21
H_2PS	$^2A''$	1.177	1.236	0.812	1.122	1.16
	$^2A'$	2.879	2.856	2.572	2.683	2.72
NH_2	$^2A_1$	2.284	2.357	1.758	2.209	2.12
PH_2	$^2A_1$	2.852	2.911	2.486	2.679	2.77
MSE		0.01	0.06	–0.35	0.03	
MUE		0.15	0.13	0.35	0.08	
MAX		–0.45	–0.26	–0.61	0.14	

[a] Estimated FCI/aug-cc-pVTZ, taken from Ref. 52.

Table 7: Calculated excitation energies (in eV) for the radical systems considered, for global double-hybrid functionals with the aug-cc-pVTZ basis set.

Compound	State	B2-PLYP	B2GP-PLYP	PBE0-DH	PBE-QIDH	Reference[a]
BH_2	$^2B_1$	1.275	1.268	1.287	1.270	1.18
HCO	$^2A''$	2.198	2.212	2.223	2.218	2.09
	$^2A'$	5.273	5.460	5.624	6.010	5.45
HOC	$^2A''$	1.105	0.988	0.998	0.969	0.92
H_2PO	$^2A''$	2.670	2.722	2.808	2.839	2.80
	$^2A'$	4.135	4.113	4.059	4.076	4.21
H_2PS	$^2A''$	1.184	1.180	1.227	1.215	1.16
	$^2A'$	2.779	2.728	2.770	2.704	2.72
NH_2	$^2A_1$	2.209	2.189	2.306	2.249	2.12
PH_2	$^2A_1$	2.847	2.859	2.918	2.916	2.77
MSE		0.03	0.03	0.08	0.10	
MUE		0.09	0.06	0.11	0.14	
MAX		0.18	0.12	0.19	0.56	

[a] Estimated FCI/aug-cc-pVTZ, taken from Ref. 52.

–Supplementary Material–

Assessing Challenging Intra- and Inter-Molecular Charge-Transfer Excitations Energies with Double-Hybrid Density Functionals

E. Brémond[a*], A. Ottochian[b], A.J. Pérez-Jiménez[c], I. Ciofini[b], G. Scalmani[d], M. J. Frisch[d], J. C. Sancho-García[c†], and C. Adamo[b,e‡]

[a] Université de Paris, ITODYS, CNRS, F-75006 Paris, France

[b] Chimie ParisTech, PSL Research University, CNRS, Institute of Chemistry for Life and Health Sciences (i-CLeHS), FRE 2027, F-75005 Paris, France

[c] Department of Physical Chemistry, University of Alicante, E-03080 Alicante, Spain

[d] Gaussian, Inc., Wallingford, 340 Quinnipiac, St., Bldg. 40, Wallingford, CT 06492, USA

[e] Institut Universitaire de France, 103 Boulevard Saint Michel, F-75005 Paris, France

*E-mail: eric.bremond@u-paris.fr
†E-mail: jc.sancho@ua.es
‡E-mail: carlo.adamo@chimie-paristech.fr

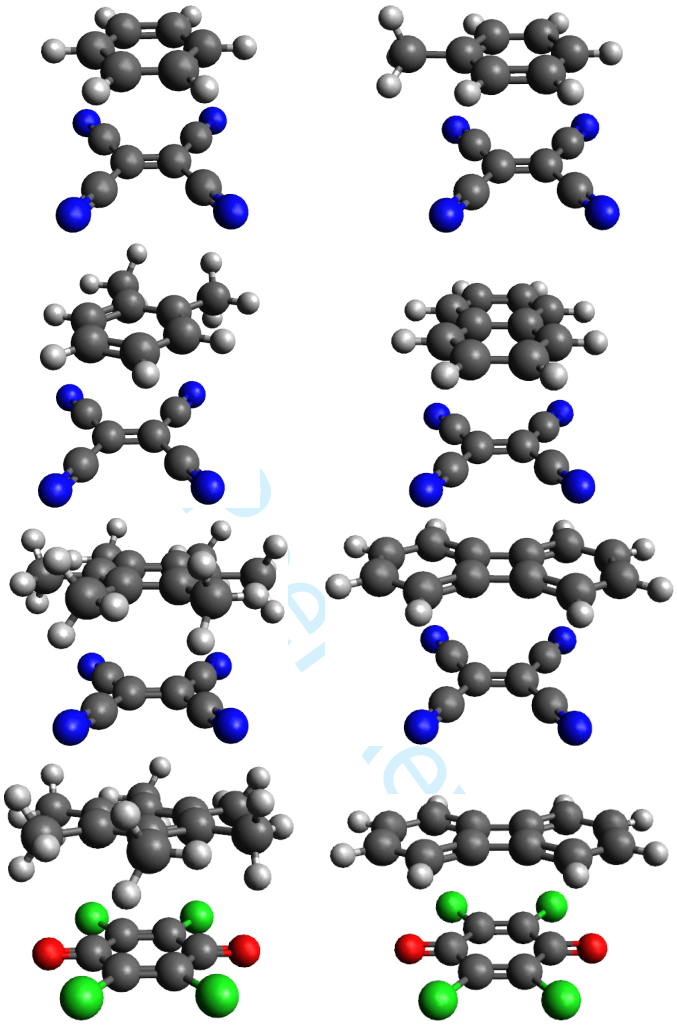

Figure 1: Relative orientation of the intermolecular complexes studied in this work (from left to right and from top to bottom): benzene-TCNE, toluene-TCNE, *o*-xylene-TCNE, naphtalene-TCNE, hexamethylbenzene-TCNE, diphenylene-TCNE, hexamethylbenzene-chloranil, and diphenylene-chloranil. Color code: C (black), H (grey), N (blue), O (red), Cl (green)

Table S1: Descriptors for the CT excited-state transitions investigated.

	B2-PLYP				B2GP-PLYP			
Compound	Ω_{POS}	Ω_{CT}	$h^+/e^-(1)$	$h^+/e^-(2)$	Ω_{POS}	Ω_{CT}	$h^+/e^-(1)$	$h^+/e^-(2)$
benzene-TCNE	1.503	0.976	0.009/0.986	0.992/0.015	1.503	0.981	0.009/0.990	0.991/0.010
toluene-TCNE	1.498	0.972	0.017/0.989	0.984/0.012	1.498	0.972	0.016/0.989	0.984/0.012
o-xylene-TCNE	1.484	0.964	0.010/0.973	0.979/0.015	1.485	0.965	0.010/0.975	0.979/0.014
naphtalene-TCNE	1.501	0.990	0.004/0.995	0.996/0.005	1.501	0.989	0.005/0.993	0.996/0.007
hexamethylbenzene-TCNE	1.516	0.953	0.008/0.961	0.992/0.040	1.514	0.958	0.008/0.966	0.992/0.035
diphenylene-TCNE	1.502	0.976	0.010/0.987	0.990/0.014	1.502	0.979	0.009/0.987	0.992/0.013
hexamethylbenzene-chloranil	1.480	0.928	0.057/0.983	0.944/0.017	1.497	0.873	0.006/0.984	0.993/0.014
diphenylene-chloranil	1.502	0.957	0.021/0.978	0.981/0.024	1.502	0.962	0.018/0.979	0.983/0.022

Table S2: Descriptors for the CT excited-state transitions investigated.

	ωB2-PLYP				ωB2GP-PLYP			
Compound	Ω_{POS}	Ω_{CT}	$h^+/e^-(1)$	$h^+/e^-(2)$	Ω_{POS}	Ω_{CT}	$h^+/e^-(1)$	$h^+/e^-(2)$
benzene-TCNE	1.504	0.975	0.009/0.987	0.991/0.013	1.504	0.977	0.010/0.987	0.991/0.013
toluene-TCNE	1.497	0.972	0.017/0.989	0.984/0.012	1.497	0.972	0.017/0.989	0.984/0.012
o-xylene-TCNE	1.486	0.965	0.010/0.976	0.979/0.014	1.502	0.975	0.011/0.986	0.990/0.015
naphtalene-TCNE	1.503	0.984	0.006/0.990	0.995/0.011	1.503	0.983	0.006/0.989	0.995/0.011
hexamethylbenzene-TCNE	1.511	0.962	0.008/0.970	0.992/0.030	1.511	0.962	0.008/0.970	0.992/0.030
diphenylene-TCNE	1.503	0.979	0.993/0.014	0.007/0.987	1.503	0.979	0.007/0.987	0.993/0.014
hexamethylbenzene-chloranil	1.502	0.974	0.012/0.986	0.989/0.015	1.502	0.974	0.011/0.985	0.989/0.015
diphenylene-chloranil	1.503	0.966	0.015/0.981	0.986/0.020	1.503	0.966	0.014/0.980	0.987/0.020

Table S3: Descriptors for the CT excited-state transitions investigated.

	PBE0-DH				PBE-QIDH			
Compound	Ω_{POS}	Ω_{CT}	$h^+/e^-(1)$	$h^+/e^-(2)$	Ω_{POS}	Ω_{CT}	$h^+/e^-(1)$	$h^+/e^-(2)$
benzene-TCNE	1.503	0.983	0.009/0.991	0.992/0.009	1.503	0.977	0.009/0.990	0.991/0.010
toluene-TCNE	1.498	0.972	0.016/0.989	0.984/0.012	1.498	0.973	0.016/0.989	0.985/0.011
o-xylene-TCNE	1.483	0.963	0.009/0.973	0.978/0.015	1.485	0.966	0.010/0.975	0.980/0.014
naphtalene-TCNE	1.500	0.991	0.004/0.995	0.996/0.005	1.501	0.989	0.004/0.993	0.996/0.007
hexamethylbenzene-TCNE	1.516	0.952	0.041/0.992	0.960/0.008	1.512	0.960	0.008/0.967	0.992/0.033
diphenylene-TCNE	1.502	0.976	0.010/0.987	0.990/0.014	1.502	0.980	0.008/0.988	0.993/0.013
hexamethylbenzene-chloranil	1.484	0.934	0.050/0.983	0.951/0.017	1.502	0.973	0.012/0.986	0.989/0.015
diphenylene-chloranil	1.501	0.957	0.021/0.978	0.981/0.023	1.457	0.976	0.011/0.992	0.988/0.009

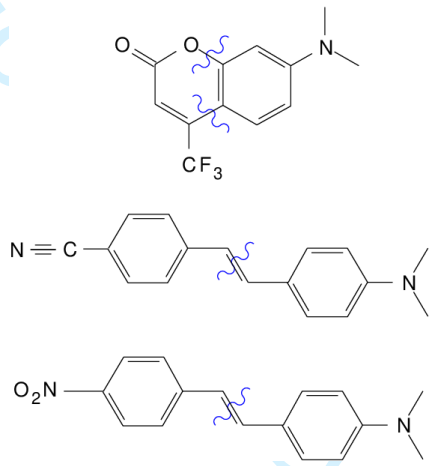

Figure 2: Sketch of the fragment separation made, with the blue lines indicating the atoms belonging to each of the fragments.

Table S4: Calculated excitation energies (in eV) with different methods and the cc-pVDZ basis set, for the ammonia-fluorine complex.

Method	$R = R_e$	$R \to \infty$
DSD-PBEP86	5.153	7.054
B2-PLYP	4.650	5.172
B2GP-PLYP	5.172	6.587
ωB2-PLYP	5.737	8.652
ωB2GP-PLYP	5.856	8.868
PBE0-DH	5.344	5.394
PBE-QIDH	5.487	7.145
RSX-0DH	6.310	9.330
RSX-QIDH	6.137	9.298
ωB97	5.549	7.688
Reference[a]	6.62	10.82

[a] CCSDT-3, taken from Ref. 1.

Table S5: Descriptors for the CT excited-state transitions of the ammonia-fluorine complex.

	$R = R_e$				$R = \infty$			
Method	Ω_{POS}	Ω_{CT}	$h^+/e^-(1)$	$h^+/e^-(2)$	Ω_{POS}	Ω_{CT}	$h^+/e^-(1)$	$h^+/e^-(2)$
B2-PLYP	1.490	0.865	0.083/0.947	0.927/0.062	1.500	1.000	0.000/1.000	1.000/0.000
B2GP-PLYP	1.483	0.854	0.094/0.945	0.912/0.061	1.500	1.000	0.000/1.000	1.000/0.000
ωB2-PLYP	1.476	0.839	0.110/0.944	0.896/0.062	1.500	1.000	0.000/1.000	1.000/0.000
ωB2GP-PLYP	1.467	0.819	0.130/0.941	0.874/0.064	1.500	1.000	0.000/1.000	1.000/0.000
PBE0-DH	1.494	0.871	0.076/0.948	0.935/0.063	1.500	1.000	0.000/1.000	1.000/0.000
PBE-QIDH	1.486	0.858	0.090/0.944	0.916/0.061	1.500	1.000	0.000/1.000	1.000/0.000

Table S6: Cartesian coordinates of benzene-TCNE dimer.

6	0.000000	1.398789	2.210379
6	0.000000	-1.398789	2.210379
6	-1.213150	0.699551	2.210679
6	1.213150	0.699551	2.210679
6	-1.213150	-0.699551	2.210679
6	1.213150	-0.699551	2.210679
1	0.000000	2.491323	2.214559
1	0.000000	-2.491323	2.214559
6	0.000000	0.686302	-1.432822
6	0.000000	-0.686302	-1.432822
6	1.220900	1.434052	-1.443795
6	-1.220900	1.434052	-1.443795
6	1.220900	-1.434052	-1.443795
6	-1.220900	-1.434052	-1.443795
7	2.204820	2.054479	-1.464782
7	-2.204820	2.054479	-1.464782
7	2.204820	-2.054479	-1.464782
7	-2.204820	-2.054479	-1.464782
1	-2.158733	1.246672	2.212219
1	2.158733	1.246672	2.212219
1	2.158733	-1.246672	2.212219
1	-2.158733	-1.246672	2.212219

Table S7: Cartesian coordinates of toluene-TCNE dimer.

6	-1.070970	-2.321680	0.000000
6	-2.381860	0.182208	0.000000
6	-1.395990	-1.695110	1.208637
6	-1.395990	-1.695110	-1.208640
6	-2.042420	-0.455960	1.205797
6	-2.042420	-0.455970	-1.205800
1	-0.573940	-3.294470	0.000000
6	1.832456	-0.145870	0.000000
6	1.209949	1.076908	0.000000
6	2.188098	-0.806300	-1.219710
6	2.188098	-0.806300	1.219710
6	0.882083	1.752188	-1.219350
6	0.882083	1.752188	1.219345
7	2.502901	-1.352370	-2.197750
7	2.502901	-1.352370	2.197749
7	0.617543	2.328197	-2.195230
7	0.617543	2.328197	2.195226
1	-1.145390	-2.174110	2.157975
1	-1.145390	-2.174110	-2.157980
1	-2.290060	0.025693	-2.155300
1	-2.290060	0.025693	2.155299
6	-3.120570	1.499082	0.000000
1	-2.883370	2.099627	0.891903
1	-2.883370	2.099627	-0.891900
1	-4.212730	1.335415	0.000000

Table S8: Cartesian coordinates of *o*-xylene-TCNE dimer.

6	0.595483	-1.963550	1.326737
6	2.199433	-0.429850	-0.415360
6	0.778276	-2.377360	0.005806
6	1.214015	-0.789610	1.773489
6	1.575310	-1.610600	-0.850230
6	2.014574	-0.011180	0.924968
1	-0.019840	-2.552050	2.011112
6	-1.879950	0.433943	0.296896
6	-1.422500	0.533009	-0.994040
6	-1.543980	1.413301	1.285898
6	-2.738430	-0.635660	0.707227
6	-0.577710	1.612040	-1.406830
6	-1.782190	-0.429310	-1.991020
7	-1.296630	2.210171	2.096786
7	-3.450990	-1.486630	1.056438
7	0.107314	2.484385	-1.759430
7	-2.073830	-1.195120	-2.816930
1	0.307507	-3.292910	-0.358520
1	1.076223	-0.468180	2.809413
1	1.727104	-1.938600	-1.882260
6	3.052881	0.374014	-1.363860
1	3.153731	-0.129590	-2.336100
1	2.619312	1.372535	-1.546910
1	4.066159	0.537587	-0.960630
6	2.670551	1.247455	1.439934
1	2.340427	2.138628	0.880252
1	2.436268	1.411607	2.501165
1	3.768190	1.201670	1.338686

Table S9: Cartesian coordinates of naphtalene-TCNE dimer.

6	-1.292310	1.840752	-1.392890
6	-1.251480	1.813917	1.416528
6	-1.733970	0.671611	-0.711120
6	-0.849120	2.943661	-0.693250
6	-1.713810	0.658339	0.725287
6	-0.828070	2.930130	0.725735
6	-2.193090	-0.485260	-1.402230
6	-2.153850	-0.511290	1.407290
6	-2.612130	-1.602910	-0.711310
6	-2.591630	-1.616240	0.707724
1	-1.311890	1.850863	-2.485860
1	-1.237810	1.802276	2.509602
1	-2.209930	-0.473270	-2.495250
1	-2.137860	-0.520380	2.500289
1	-2.963240	-2.482640	-1.254730
1	-2.926910	-2.506260	1.244356
6	1.912581	-0.750670	-0.695090
6	1.916945	-0.720170	0.677407
6	2.382526	0.358211	-1.469360
6	1.456055	-1.898190	-1.419070
6	2.390657	0.422577	1.398110
6	1.467725	-1.835120	1.454983
7	2.773413	1.242050	-2.117130
7	1.101264	-2.824960	-2.026370
7	2.784301	1.335540	2.002312
7	1.122538	-2.733820	2.108279
1	-0.473300	3.808418	1.269033
1	-0.509700	3.832136	-1.229860

Table S10: Cartesian coordinates of hexamethylbenzene-TCNE dimer.

C	1.526348	2.528794	1.460000
C	1.526348	1.221096	0.705000
C	1.526348	0.000000	1.410000
C	1.526348	-1.221096	0.705000
C	1.526348	-1.221096	-0.705000
C	1.526348	0.000000	-1.410000
C	1.526348	1.221096	-0.705000
C	1.526348	0.000000	2.920000
C	1.526348	-2.528794	1.460000
C	1.526348	-2.528794	-1.460000
C	1.526348	0.000000	-2.920000
C	1.526348	2.528794	-1.460000
H	1.526348	1.027663	3.283329
H	2.416330	-0.513832	3.283329
H	0.636366	-0.513832	3.283329
H	1.526348	3.357278	0.751682
H	2.416330	2.586531	2.086656
H	0.636366	2.586531	2.086656
H	1.526348	2.329615	-2.531647
H	2.416330	3.100362	-1.196673
H	0.636366	3.100362	-1.196673
H	1.526348	-1.027663	-3.283329
H	2.416330	0.513832	-3.283329
H	0.636366	0.513832	-3.283329
H	1.526348	-3.357278	-0.751682
H	2.416330	-2.586531	-2.086656
H	0.636366	-2.586531	-2.086656
H	1.526348	-2.329615	2.531647
H	2.416330	-3.100362	1.196673
H	0.636366	-3.100362	1.196673
C	1.933652	0.000000	0.685000
C	1.933652	0.000000	-0.685000
C	1.933652	-1.219275	1.432173
N	1.933652	-2.208338	2.038271
C	1.933652	1.219275	1.432173
N	1.933652	2.208338	2.038271
C	1.933652	1.219275	-1.432173
N	1.933652	2.208338	-2.038271
C	1.933652	-1.219275	-1.432173
N	1.933652	-2.208338	-2.038271

Table S11: Cartesian coordinates of diphenylene-TCNE dimer.

C	-0.750110	1.667780	0.710680
C	0.749649	1.668097	0.710421
C	0.749404	1.668266	-0.710281
C	-0.750355	1.667949	-0.710022
C	-1.912342	1.668028	-1.435089
C	-1.911846	1.667684	1.436147
C	1.911636	1.668493	1.435487
C	1.911141	1.668836	-1.435748
C	-3.116169	1.667361	0.684632
C	-3.116404	1.667524	-0.683158
C	3.115463	1.668842	-0.684233
C	3.115699	1.668678	0.683557
H	-1.912548	1.668259	-2.525089
H	-4.068917	1.667594	-1.215335
H	-4.068497	1.667303	1.217137
H	-1.911676	1.667655	2.526147
H	1.911842	1.668463	2.525487
H	4.068211	1.669023	1.215733
H	4.067791	1.669314	-1.216738
H	1.910970	1.669067	-2.525748
C	0.685419	-1.981812	-0.000355
C	-0.684580	-1.982101	-0.000118
C	-1.431984	-1.981932	-1.219243
C	1.432821	-1.981617	1.218769
C	1.432401	-1.981326	-1.219737
C	-1.431563	-1.982223	1.219263
N	-2.037435	-1.982769	2.208485
N	2.039035	-1.981906	2.207781
N	2.038273	-1.981379	-2.208959
N	-2.038196	-1.982241	-2.208255

Table S12: Cartesian coordinates of hexamethylbenzene-chloranil dimer.

C	-1.270434	1.455159	-0.674994
C	-0.704990	-2.204838	-1.221110
C	-1.459980	-2.204832	-2.528814
C	0.705010	-2.204838	-1.221099
C	1.410000	-2.204843	0.000002
C	0.704991	-2.204847	1.221092
C	-0.705009	-2.204848	1.221081
C	-1.409999	-2.204843	-0.000020
C	-1.270434	1.455153	0.675006
C	-0.000000	1.455150	1.453529
C	1.270433	1.455154	0.675006
C	1.270433	1.455159	-0.674993
C	-0.000000	1.455162	-1.453516
C	2.920000	-2.204843	0.000013
C	1.459981	-2.204852	2.528796
C	-1.460019	-2.204855	2.528774
C	-2.919999	-2.204844	-0.000031
C	1.460020	-2.204833	-2.528792
O	-0.000000	1.455144	2.663529
Cl	2.688039	1.455150	1.613299
Cl	2.688039	1.455164	-1.613287
O	-0.000000	1.455166	-2.663516
Cl	-2.688039	1.455162	-1.613286
Cl	-2.688039	1.455149	1.613299
H	-0.751656	-2.204828	-3.357293
H	-2.086636	-3.094814	-2.586559
H	-2.086636	-1.314850	-2.586551
H	2.531665	-2.204832	-2.329605
H	1.196697	-1.314847	-3.100358
H	1.196697	-3.094812	-3.100366
H	3.283322	-2.204848	1.027679
H	3.283334	-1.314858	-0.513812
H	3.283334	-3.094823	-0.513820
H	0.751657	-2.204855	3.357275
H	2.086637	-3.094834	2.586533
H	2.086636	-1.314870	2.586540
H	-2.531664	-2.204852	2.329587
H	-1.196695	-3.094838	3.100340
H	-1.196696	-1.314873	3.100347
H	-3.283321	-2.204841	-1.027697
H	-3.283332	-3.094828	0.513794
H	-3.283333	-1.314863	0.513801

Table S13: Cartesian coordinates of diphenylene-chloranil dimer.

C	-0.000000	1.453523	0.000000
C	-1.270434	0.675000	0.000000
C	-1.270434	-0.674999	-0.000000
C	-0.000000	-1.453522	-0.000000
C	1.270433	-0.674999	-0.000000
C	1.270433	0.674999	-0.000000
Cl	-2.688040	1.613293	0.000000
Cl	-2.688040	-1.613292	-0.000000
O	-0.000000	-2.663523	0.000000
Cl	2.688039	-1.613292	-0.000001
Cl	2.688039	1.613292	-0.000001
O	-0.000000	2.663523	0.000000
C	-0.683256	-3.116292	3.520000
C	-1.435968	-1.912205	3.520000
C	-0.710198	-0.750242	3.520000
C	0.710198	-0.750242	3.519999
C	1.435968	-1.912205	3.519999
C	0.683256	-3.116292	3.519999
C	-0.710197	0.750241	3.520000
C	0.710199	0.750241	3.519999
C	1.435969	1.912204	3.519999
C	0.683257	3.116291	3.519999
C	-0.683255	3.116291	3.520000
C	-1.435967	1.912204	3.520000
H	2.525290	1.912193	3.520000
H	1.215538	4.068563	3.520000
H	-1.215536	4.068563	3.520000
H	-2.525288	1.912193	3.520001
H	-2.525288	-1.912193	3.520001
H	-1.215536	-4.068563	3.520000
H	1.215537	-4.068563	3.519999
H	2.525289	-1.912193	3.519999

Table S14: Cartesian coordinates of Coumarin-152.

C	-3.558714	-0.762996	0.349325
C	-3.550910	0.683210	0.288106
C	-2.409629	-1.489510	0.282792
O	-2.287052	1.287268	0.150528
C	-1.133309	-0.849809	0.148538
C	-1.127274	0.562554	0.086713
C	0.120049	-1.494642	0.068031
C	0.040771	1.298044	-0.044352
C	1.293212	-0.783612	-0.061265
C	1.284587	0.638646	-0.116597
H	-4.529332	-1.229549	0.450766
O	-4.513940	1.414935	0.339536
H	0.167323	-2.576906	0.106451
H	-0.042140	2.376397	-0.088663
H	2.229523	-1.324617	-0.120848
C	-2.489131	-2.998739	0.354417
F	-1.791757	-3.486017	1.418623
F	-3.757792	-3.450965	0.474751
F	-1.964877	-3.581468	-0.759871
N	2.452326	1.346369	-0.234332
C	2.415266	2.799557	-0.334979
H	1.916256	3.239044	0.537166
H	3.438454	3.174301	-0.369876
H	1.887831	3.130402	-1.240386
C	3.723210	0.649551	-0.391321
H	4.518557	1.391303	-0.467254
H	3.932586	0.006674	0.472476
H	3.735907	0.030577	-1.298476

Table S15: Cartesian coordinates of DCS.

C	-4.200538	1.260897	-0.075070
C	-5.574871	1.097678	-0.003576
C	-6.119025	-0.177789	0.226656
C	-5.249694	-1.275874	0.381772
C	-3.879585	-1.099604	0.308238
C	-3.313341	0.173919	0.077617
C	-1.884082	0.416711	-0.008916
C	1.120858	0.968481	-0.197737
C	0.527820	-0.290519	0.031324
C	1.405144	-1.381831	0.185052
C	2.781742	-1.243087	0.117567
C	3.367250	0.023783	-0.112564
C	2.492029	1.128881	-0.268659
C	-0.902038	-0.509514	0.113908
N	4.732180	0.180643	-0.182695
C	5.307437	1.495563	-0.420509
C	5.606668	-0.970130	-0.018958
H	-3.789509	2.251331	-0.253481
H	-6.238374	1.947873	-0.123983
C	-7.530423	-0.359556	0.302438
H	-5.666915	-2.261809	0.559632
H	-3.235066	-1.964142	0.431648
H	-1.609843	1.454898	-0.190883
H	0.493035	1.845914	-0.323836
H	0.985614	-2.369636	0.363299
H	3.406730	-2.119579	0.243600
H	2.895060	2.119276	-0.446806
H	-1.186175	-1.545900	0.295894
H	4.975389	1.917541	-1.373261
H	5.031317	2.207056	0.362811
H	6.393952	1.403819	-0.440212
H	5.420670	-1.726356	-0.800671
H	5.477897	-1.430117	0.975715
H	6.642038	-0.639281	-0.107487
N	-8.683217	-0.508999	0.364498

Table S16: Cartesian coordinates of DNAS.

C	-3.973931	1.323544	-0.044092
C	-5.350402	1.173229	0.017234
C	-5.878294	-0.105128	0.193953
C	-5.050235	-1.225001	0.308953
C	-3.678055	-1.059282	0.245825
C	-3.099630	0.218984	0.067559
C	-1.669573	0.450181	-0.005571
C	1.341651	0.972488	-0.164012
C	0.732761	-0.287893	0.012948
C	1.596211	-1.395936	0.125372
C	2.973931	-1.271664	0.067275
C	3.575674	-0.003332	-0.110463
C	2.714372	1.118439	-0.224676
C	-0.698160	-0.492803	0.082807
N	4.941603	0.139153	-0.170482
C	5.534666	1.455333	-0.353958
C	5.802271	-1.028001	-0.050554
H	-3.549992	2.314914	-0.181587
H	-6.023260	2.018158	-0.068047
N	-7.330868	-0.278864	0.260567
H	-5.500155	-2.201317	0.445360
H	-3.041676	-1.933722	0.335937
H	-1.382679	1.491395	-0.145093
H	0.724687	1.861715	-0.256578
H	1.163442	-2.384483	0.262785
H	3.588006	-2.159847	0.159799
H	3.130603	2.109840	-0.361937
H	-0.995625	-1.531880	0.222387
H	5.197922	1.905771	-1.309752
H	5.253122	2.130343	0.479664
H	6.619796	1.350075	-0.374223
H	5.604132	-1.753658	-0.851041
H	5.658605	-1.532044	0.914803
H	6.841700	-0.706117	-0.123016
O	-8.039513	0.731475	0.155630
O	-7.769108	-1.426595	0.418127

Table S17: Cartesian coordinates of the ammonia-fluorine complex at $R = R_e$.

H	2.49067	0.939499	-0.000156
N	2.08528	0.000000	0.000003
H	2.49073	-0.469633	0.813668
H	2.49062	-0.469860	-0.813586
F	-0.22296	0.000000	0.000001
F	-1.71040	0.000000	0.000000

References

[1] Kozma, B.; Berraud-Pache, R.; Tajti, A.; Szalay, P. G. Potential energy surfaces of Charge Transfer states. *Molecular Physics* **2020**, *118*, e1776903.